MARTIN MARIETTA ENERGY SYSTEMS LIBRARIES
3 4456 0050957 2

cy. 4

ORNL-4685
UC-48 — Biology and Medicine

OAK RIDGE NATIONAL LABORATORY
CENTRAL RESEARCH LIBRARY
DOCUMENT COLLECTION
LIBRARY LOAN COPY
DO NOT TRANSFER TO ANOTHER PERSON
If you wish someone else to see this document, send in name with document and the library will arrange a loan.

ANALYSIS OF ROUND, TURBULENT, BUOYANT JETS DISCHARGED TO FLOWING STRATIFIED AMBIENTS

E. A. Hiser

OAK RIDGE NATIONAL LABORATORY
operated by
UNION CARBIDE CORPORATION
for the
U.S. ATOMIC ENERGY COMMISSION

Printed in the United States of America. Available from
National Technical Information Service
U.S. Department of Commerce
5285 Port Royal Road, Springfield, Virginia 22151
Price: Printed Copy $3.00; Microfiche $0.95

This report was prepared as an account of work sponsored by the United States Government. Neither the United States nor the United States Atomic Energy Commission, nor any of their employees, nor any of their contractors, subcontractors, or their employees, makes any warranty, express or implied, or assumes any legal liability or responsibility for the accuracy, completeness or usefulness of any information, apparatus, product or process disclosed, or represents that its use would not infringe privately owned rights.

ORNL-4685

Contract No. W-7405-eng-26

DIRECTOR'S DIVISION

ANALYSIS OF ROUND, TURBULENT, BUOYANT JETS DISCHARGED TO FLOWING STRATIFIED AMBIENTS

E. A. Hirst

JUNE 1971

OAK RIDGE NATIONAL LABORATORY
Oak Ridge, Tennessee
operated by
UNION CARBIDE CORPORATION
for the
U.S. ATOMIC ENERGY COMMISSION

MARTIN MARIETTA ENERGY SYSTEMS LIBRARIES
3 4456 0050957 2

CONTENTS

Nomenclature v

Abstract 1

1. Introduction 1

2. Historical Background 2

   2.1 Class 1 Flows 3

   2.2 Buoyant Jets Discharged at Arbitrary Angles to the Vertical 5

   2.3 Nonbuoyant Jets Discharged to a Cross Flow 6

   2.4 Buoyant Jets Discharged to a Cross Flow 7

   2.5 Summary 8

3. Derivation of the Integral Equations 9

   3.1 The Basic Equations 9

   3.2 The Integral Equations 11

   3.3 Summary 12

4. Integral Method Solution 12

   4.1 Velocity and Density Difference Profiles 12

   4.2 Generalized Entrainment Functions 14

   4.3 Comparison With Experiments 15

   4.4 Summary 24

5. Applications of the New Method 24

6. Summary and Recommendations 28

   6.1 Future Experimental Study 28

   6.2 Future Theoretical Analysis 29

Appendix A: The s, r, ϕ Coordinate System 29

Appendix B: The Basic Equations in Terms of s, r, ϕ 31

Appendix C: Derivation of the Axisymmetric Equations 32

Appendix D: Specification of the Initial Conditions 34

References 35

NOMENCLATURE

a_i	dimensionless coefficients in the entrainment equation
b	measure of the jet width
c	concentration
c_v, c_p	specific heat at constant volume and at constant pressure, respectively
C_D	drag coefficient
C_i	$\cos\theta_i$
$C\phi$	$\cos\phi$
D	mass diffusivity
e	shorthand notation for $(r/\rho_1)\, C\phi C_2 + (r/\rho_2) S\phi$
E	entrainment rate
F	body force
F_D	drag force
Fr	Froude number, $u_0^2/[(\rho_\infty - \rho_0)\, r_0 g/\rho_0]$, dimensionless
Fr_L	local Froude number, $u_m^2/[(\rho_\infty - \rho_m)\, bg/\rho_0]$, dimensionless
g	acceleration of gravity, 32.174 ft/sec^2
$\mathbf{g}$	gravity vector, $-g\mathbf{k}$
$\mathbf{i}, \mathbf{j}, \mathbf{k}$	unit vectors parallel to the x, y, z axes, respectively
$\mathbf{i}_s, \mathbf{i}_r, \mathbf{i}_\phi$	unit vectors parallel to the s, r, ϕ axes, respectively
I	similarity integral, $-\int_0^\infty (u/u_m)\, [\partial(r\, \overline{u'v'}/u_m^2)/\partial r]\, d(r/b)$
k	thermal conductivity
p	pressure
p^*	difference between local pressure and hydrostatic pressure
q	$\int_0^\infty \bar{u}^2 r\, dr - 1/4\, E^2 - 1/4 \lim_{r\to\infty} (r^2 \bar{v}'^2)$
r	radial distance from jet center line
$r_{0.5}$	jet half-width; distance from center line to point at which $u/u_m = 0.5$
R	velocity ratio, u_∞/u_0
R_{12}	$R \cdot \sin\theta_1 \cdot \cos\theta_2$
s	streamwise coordinate, distance along the jet axis
S_i	$\sin\theta_i$
$S\phi$	$\sin\phi$
t	temperature
T	stratification parameter, $(\rho_\infty - \rho_0)/[-r_0(d\rho_\infty/dz)]$
u	component of velocity parallel to $\mathbf{i}_s$
u_{12}	$u_\infty \cdot \sin\theta_1 \cdot \cos\theta_2$
v	component of velocity parallel to $\mathbf{i}_r$
$\mathbf{v}$	vector velocity, $u\mathbf{i}_s + v\mathbf{i}_r + w\mathbf{i}_\phi$
$\dot{V}$	volume flow rate, $\pi r^2 u$
w	component of velocity parallel to $\mathbf{i}_\phi$
x	Cartesian coordinate, horizontal and perpendicular to free stream
y	Cartesian coordinate, horizontal and parallel to free stream
z	Cartesian coordinate, positive vertically up
β	thermal coefficient of volumetric expansion, $-(1/\rho_0)\, (\partial\rho/\partial t)_p$

γ	concentration coefficient of volumetric expansion, $-(1/\rho_0)\,(\partial\rho/\partial c)_t$
ϵ_m, ϵ_h	eddy diffusivities for momentum and heat, respectively
θ_1	angle between the projection of $\mathbf{i}_s$ onto the x, y plane and the x axis
θ_2	angle between $\mathbf{i}_s$ and the x, y plane
λ	spreading ratio between density and velocity profiles
ν	kinematic viscosity
ρ	density
ρ_1	radius of curvature, $(d\theta_1/ds)^{-1}$
ρ_2	radius of curvature, $(d\theta_2/ds)^{-1}$
τ	time
ϕ	azimuthal angle
Φ	dissipation function
$(\ )_o$	at diffuser outlet, $s = 0$
$(\ )_m$	at jet center line, $r = 0$
$(\ )_{th}$	top-hat value
$(\ )_\infty$	free stream value
$(\ )_e$	at end of flow establishment zone
$\overline{(\ )}$	average with respect to time
$(\ )'$	fluctuating component
$\Delta(\ )$	$(\ ) - (\ )_\infty$

ANALYSIS OF ROUND, TURBULENT, BUOYANT JETS DISCHARGED TO FLOWING STRATIFIED AMBIENTS

E. A. Hirst

ABSTRACT

Modern steam electric power plants discharge approximately 1.5 to 2 kWhr of waste heat for every kWhr of electrical energy produced. Usually this heat is discharged to an adjacent water body in "once-through" cooling which increases the water temperature near the outfall. Since aquatic organisms tend to be temperature-sensitive, these thermal additions modify the local aquatic environment.

In order to assess the ecological consequences of waste heat discharge one must first know the physical changes (temperature, velocity, salinity) induced by these discharges. It is with this latter aspect, prediction of physical properties, that the current work is primarily concerned.

A new integral method is devised to predict the development of a momentum jet discharged to an infinite ambient through a single circular submerged diffuser. The jet is subjected to buoyancy forces, ambient cross flows, ambient turbulence, and ambient density stratification and will, in general, follow a three-dimensional path.

This method differs from existing methods in several ways. First, the new method is applicable to a much wider range of flows. For example, the new method can handle flows for which the trajectories are three-dimensional, whereas existing methods are limited to jets with two-dimensional paths.

Second, the method is based on an integration of the basic partial differential equations written in a new "natural" coordinate system. Deriving the integral equations from these basic equations reveals certain terms involving the turbulence and radius of curvature which do not appear in the older methods.

Third, a new entrainment function has been postulated. This function includes the effects of internal turbulence, buoyancy, and cross flow. This new equation contains four coefficients, only one of which must be determined empirically by fitting the predictions to the data.

The theoretical predictions have been compared with data for 100 different flows, and the agreement between theory and experiment is good. This is especially significant since the method has been used to predict a wide range of flows with *all* the entrainment coefficients kept constant.

Finally, the new method is used to assess the physical consequences of thermal discharges from a hypothetical power plant. This example shows how the new method can be used to help design optimal discharge systems.

1. INTRODUCTION

This work is concerned with the behavior of momentum jets discharged to an infinite ambient through a single circular submerged diffuser subjected to buoyancy forces, ambient cross flows, ambient turbulence, and ambient density stratification. The primary objectives of this work are to: (1) derive the basic equations (mass, momentum, energy, and concentration) governing the development of jets with three-dimensional trajectories using a new "natural" coordinate system which moves with the center line of the jet; and (2) develop a simple integral method solution to these basic equations. This latter effort involves the formulation of a generalized entrainment function which accounts for all the effects listed above. Results obtained with the integral method are compared with data from about 100 different jet and plume experiments covering a wide range of the variables. The agreement between theory and experiment is good.

This research is motivated by a concern with the ecological consequences of thermal effluents from steam-electric power plants.* Modern power plants discharge approximately 1.5 to 2 times as much thermal energy (waste heat) as electrical energy is produced. Usually this heat is discharged to an adjacent water body in "once-through" cooling which increases the water temperature near the outfall. Aquatic organisms tend to be temperature-sensitive; hence these thermal additions can modify the local ecosystem.

As part of the power plant site selection process one must assess the ecological consequences of the thermal discharges. If the ecological impact is unacceptable, then alternative means of waste heat discharge can be employed, for example, cooling towers.

*However, the theory developed here is general enough to be applicable to other problems of current interest, for example, brine effluents from desalination plants and smokestack plumes.

In order to predict the ecological impact of such thermal additions one must first predict the physical changes (temperature, salinity, velocity) due to the thermal discharges. It is with this latter aspect – theoretical predictions of physical properties – that the current work is concerned.

The waste heat can be discharged to the receiving water body in many ways, for example, single submerged diffuser, multiport submerged diffuser, or surface jet. This study is limited to a consideration of discharge through a single circular submerged diffuser. In addition, the theoretical development assumes that the receiving water body is infinite in extent, and this excludes the influences of shoreline, bottom topography, and the air/water interface. Extensions of this research will remove some of these limitations.

The engineering model developed here can be coupled with biological models (which predict organism behavior given their time-temperature history) to produce an integrated model capable of predicting certain ecological consequences of waste heat discharge through a single submerged diffuser given the conditions at the diffuser exit and the ambient conditions.

Chapter 2 reviews previous experimental and theoretical efforts related to buoyant jets. A large body of experimental data exists for flows in which the trajectory of the jet remains in a single plane. Data for flows with three-dimensional trajectories are nonexistent. Similarly, several theoretical methods exist for the prediction of single-plane trajectory jets. But none of these methods are capable of predicting the growth and development of jets with three-dimensional trajectories. The method developed here is concerned with buoyant jets whose trajectories are not confined to a single plane, an extension and logical outgrowth of previous efforts.

In Chap. 3 the basic partial differential equations governing the development of a buoyant jet are derived in a new "natural" coordinate system which moves with the jet center line. The resulting equations and boundary conditions are extremely complicated. Therefore, the equations are simplified by assuming the flow to be axisymmetric and then integrating these equations over a cross section of the jet. This yields a set of "integral" equations with the steamwise coordinate as the single independent variable.

Chapter 4 develops the solution to these integral equations. In order to achieve closure, velocity and density profiles and an entrainment function must be assumed. Gaussian profiles are used. A generalized entrainment function is formulated which includes the effects of internal turbulence, buoyancy, and cross flow. This new entrainment function contains four coefficients, only one of which must be determined empirically by fitting predictions to the data.

The theoretical predictions are compared with data for 100 different flows. The agreement between theory and experiment is good, which is especially significant since the method has been used to predict a wide range of flows with *all* the entrainment coefficients kept constant.

The method developed in Chaps. 3 and 4 is capable of predicting the temperature and velocity fields in buoyant jets discharged at arbitrary angles to flowing stratified ambients. In Chap. 5 this method is used to study the thermal discharge from a hypothetical 1000-MW(e) power plant sited on the Gulf of California. Jet trajectories and temperature fields are computed for 24 different discharge configurations. These cases include two flow-rate–temperature-difference combinations and various initial jet orientations for jets discharged to both quiescent and flowing ambients. The results of these computations are discussed in terms of jet location, dilution, and size of the mixing zone. Ways in which this method can be used to develop optimal thermal discharge systems are described.

The last chapter discusses the significance and limitations of the present method. The possibilities for future research are also described.

2. HISTORICAL BACKGROUND

Two excellent reviews of submerged jet theory and experiment have been published by Silberman and Stefan[1] and Baumgartner and Trent.[2] Therefore we shall discuss only those aspects of jet flow applicable to the study reported in Chaps. 3, 4, and 5.

Jet flows can be divided into several classes according to the trajectory of the jet center line:

Class 1. Straight line trajectories
- *a.* simple momentum jets
- *b.* momentum jets discharged to a coflowing stream
- *c.* vertically discharged buoyant jets and plumes*

Class 2. Single plane trajectories
- *a.* buoyant jets discharged at arbitrary angles to the vertical

*High Froude number flows are usually referred to as jets, low Froude number flows are called plumes, and intermediate flows are called buoyant jets or forced plumes.

b. nonbuoyant jets discharged to a cross flow

c. buoyant jets discharged in the plane formed by the cross-flow vector and the gravity force ($\mathbf{u}_0 \perp \mathbf{g} \times \mathbf{u}_\infty$)

Class 3. Three-dimensional trajectories

a. buoyant jets discharged at arbitrary angles to a free stream

For all three classes the jet passes through several regimes as it moves from the outfall through the ambient. The three regimes commonly considered are (see Fig. 1):

1. *Zone of flow establishment,* in which the velocity and turbulence profiles undergo a transition from their internal flow shapes to a free turbulent flow condition. It is in this region that mixing begins with the ambient fluid. Here the flow is strongly influenced by the outfall conditions and only slightly influenced by ambient conditions.

2. *Zone of established flow* begins when turbulent mixing has reached the jet center line. In this region the profiles have assumed their free turbulent shapes and the jet dynamics are governed by the jet's momentum and buoyancy and the free-stream conditions, but not by the initial outfall conditions.

3. *Field zone,* in which the jet momentum is depleted and the jet fluid is convected and diffused by the ambient currents and ambient turbulence.

In what follows we shall be primarily concerned with region 2, the zone of established flow. The zone of flow establishment is short (10 to 20 r_0) relative to the zone of established flow, and by the time the fluid has reached the field zone the concentration and temperature excess are small relative to their values in region 2.

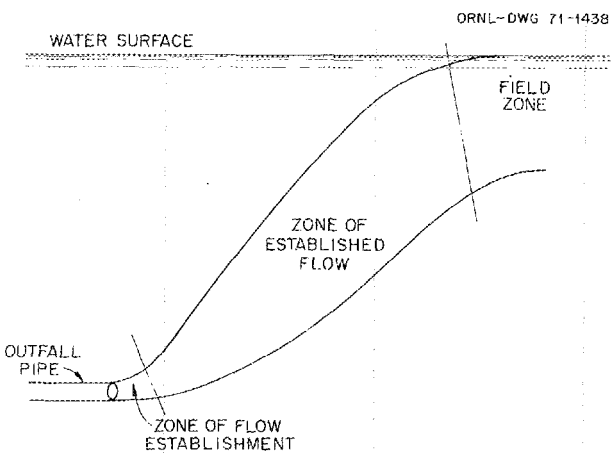

Fig. 1. Flow regimes for buoyant jets.

2.1 Class 1 Flows

Simple momentum jets (Fr = ∞) have been studied extensively during the past 40 years as a classic example of nonisotropic free turbulence. The experimental work of Albertson et al.[3] showed that the mean velocity profile is very nearly Gaussian, that is,

$$u/u_m = e^{-76r^2/x^2}$$

or

$$u/u_m = e^{-r^2/b^2} , \tag{1}$$

where $b = x/\sqrt{76}$ is a measure of the jet width.

Albertson also showed that the center line velocity decayed as

$$u_m/u_0 = 12.4r_0/x \tag{2}$$

beyond the zone of flow establishment, which was found to be $12.4r_0$ in length. The rate at which ambient fluid is entrained into the jet, E, was shown to be

$$E = 0.057u_m b . \tag{3}$$

In recent years the work of Albertson has been significantly extended by Sami et al.,[4] Becker et al.,[5] and Wygnanski et al.[6] Sami conducted a detailed investigation of the mean and turbulent flow fields within the region of flow establishment. Wygnanski made similar measurements in the fully developed flow region.

Becker investigated the concentration field in a simple momentum jet. The profiles of concentration (or any other scalar property) are also Gaussian but slightly flatter than are the velocity profiles:

$$c/c_m = e^{-61.6r^2/x^2}$$

or

$$c/c_m = e^{-(r/\lambda b)^2} , \tag{4}$$

where λ ($= \sqrt{76/61.6} = 1.11$ for a simple momentum jet) is a measure of the relative spreading of the concentration and velocity profiles. Also, the center line concentration decays somewhat more rapidly than does the center line velocity, that is,

$$c_m/c_0 = 10.8\, r_0/x . \tag{5}$$

Forstall and Shapiro[7] and Landis and Shapiro[8] investigated the mechanics of nonbuoyant turbulent jets discharged to a coflowing ambient. The free stream tends to narrow the jet and delay the onset of the fully developed flow region. However, the center line velocity and concentration in the established flow region decay with x^{-1}, as they do for simple momentum jets.

Reviews of theoretical analyses for simple momentum jets and jets in a coflowing stream can be found in Hinze[9] and Abramovich.[10]

The work of Rouse et al.[11] on vertical plumes was concerned with the velocity and temperature fields above a point heat source. Their measurements showed that the velocity and temperature profiles for these low Froude number flows were also Gaussian:

$$u/u_m = e^{-96r^2/x^2}$$

or

$$u/u_m = e^{-r^2/b^2} , \tag{6}$$

where $b = x/\sqrt{96}$ at low Froude numbers, and

$$\Delta t/\Delta t_m = e^{-71r^2/x^2}$$

or

$$\Delta t/\Delta t_m = e^{-(r/\lambda b)^2} , \tag{7}$$

where $\lambda = \sqrt{96/71} = 1.16$ for these flows.

Because

$$\lambda_{Fr=0} = 1.16$$

and

$$\lambda_{Fr=\infty} = 1.11 , \tag{8}$$

scalar properties diffuse more rapidly relative to the velocity for low Fr flows than for high Fr flows.

Rouse's measurements also showed that the center line velocity decayed as $x^{-1/3}$ and the center line temperature decayed as $x^{-5/3}$ rather than as x^{-1}. Abraham[12] suggested that, for low Fr flows, the entrainment rate is

$$E = 0.085 u_m b . \tag{9}$$

A comparison with Eq. (3) shows that the entrainment is higher for plumes than for jets. Abraham[13] also showed that the zone of flow establishment becomes shorter with decreasing Fr.

Abraham[14] and Frankel and Cumming[15] measured the center line concentration in vertical buoyant jets discharged with various Froude numbers. It is difficult to draw conclusions from their raw data because each data point represents a different flow, at a different Fr. However, Frankel and Cumming made enough measurements to permit cross-plotting the data, from which curves of c_m/c_o vs z/r_o for particular Fr were obtained. These curves indicate that the concentration at any height (z/r_o) increases with increasing Fr. This is probably due to the higher entrainment rate for low Froude number flows.

Several investigators have studied the discharge of vertical plumes to a stratified ambient, in which the free-stream density decreases with increasing height. For such a stably stratified ambient the buoyant jet will only reach a certain height, determined by its initial Froude number and the degree of stratification. Experimental height of rise data for vertical buoyant jets were given by Hart,[16] Crawford and Leonard,[17] Abraham and Eysink,[18] Fox,[19] and Fan.[20]

Several theories exist for the prediction of vertically discharged buoyant jets, all of which are based on the integrated equations of motion. The methods of Rouse et al.,[11] Priestley and Ball,[21] and Schmidt[22] involve a solution to the integral conservation equations of vertical momentum, mechanical energy, and diffusion (energy):

$$\frac{d}{dz}\left(\int_0^\infty ru^2\,dr\right) = -\int_0^\infty r\frac{\Delta\rho}{\rho_0}g\,dr , \tag{10}$$

$$\frac{d}{dz}\left(\int_0^\infty \frac{1}{2}ru^3\,dr\right) = -\int_0^\infty ru\frac{\Delta\rho}{\rho_0}g\,dr + \int_0^\infty r\overline{u'v'}\frac{\partial u}{\partial r}\,dr , \tag{11}$$

$$\frac{d}{dz}\left(\int_0^\infty ru\,\Delta\rho\,dr\right) = -\frac{d\rho_\infty}{dz}\int_0^\infty ru\,dr . \tag{12}$$

The shear stress integral in Eq. (11) is assumed to be similar and known. The velocity and density difference profiles are taken to be either Gaussian or "top-hat." See Fig. 2 for a comparison of the two profile shapes. The theoretical results are identical regardless of which profile shape is used, provided that

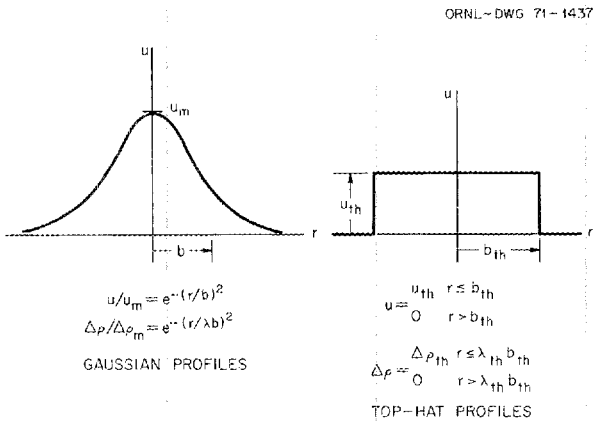

Fig. 2. Velocity and density difference profile shapes.

$$\lambda_{th} = \sqrt{\frac{\lambda_G^2 + 1}{2}}\,, \tag{13}$$

and

$$a_{th} = \sqrt{2}\, a_G\,, \tag{14}$$

where

$$E_{th} = a_{th}\, u_{th}\, b_{th} \text{ and } E_G = a_G u_m b\,, \tag{15}$$

and $u_{th} = u_m/2$ is the average jet velocity and $b_{th} = \sqrt{2}b$ is a characteristic jet width.*

Morton et al.[23] also solved this problem using the integral method. However, they dropped the mechanical energy equation and used instead the integral form of mass conservation:

$$\frac{d}{dz}\left(\int_0^\infty ru\, dr\right) = E\,. \tag{16}$$

In order to evaluate the integrals they used the top-hat profiles, with the entrainment function:

$$E = a u_{th} b_{th},$$

with $a = \sqrt{2}(0.085)$, the value appropriate for plumes.

Fox[19] developed an interesting and valuable method for determining plume development in a stratified or uniform ambient. Using the integral equations for conservation of mass, momentum, mechanical energy, and energy and Gaussian profiles for the velocity and density, he *derived* an entrainment equation:

$$E = (a_1 + a_2/Fr_L)u_m b\,, \tag{17}$$

where Fr_L is the local Froude number. This entrainment function is a generalization of Morton's formulation. According to Fox:

> . . . . the entrainment relationship did not require any external specification other than the assumption of similarity common to all plume theories, and the added assumption of a similarly distributed $(\overline{u'v'})$. Actually, the entrainment relationship is the result of requiring the four differential equations in the three dependent variables to be consistent . . . .

With Eq. (17) the entrainment coefficient increases for decreasing Fr_L, which is in agreement with experimental observations. Also, for stratified flows Fr_L becomes negative as the plume rises above its equilibrium height. Thus E may become negative, and this provides theoretical solutions which are physically more realistic than ones obtained with a constant entrainment coefficient.

The mechanical energy integral equation is used again in Chap. 4 to derive an entrainment function for buoyant jets discharged with arbitrary initial orientation.

2.2 Buoyant Jets Discharged at Arbitrary Angles to the Vertical

Nonvertical buoyant jets discharged to a uniform quiescent ambient have been experimentally studied by Cederwall[24] (cited in Abraham[13]), Bosanquet et al.,[25] Frankel and Cumming,[15] Anwar,[26] and Fan.[20]

Cedarwall measured the center line location and concentration for various horizontally discharged jets. Unfortunately, each data point was obtained with different initial conditions, making it difficult to draw conclusions from his data. Frankel and Cumming measured the center line concentration for buoyant jets discharged at angles of 0, 15, 30, 45, and 90° to the horizontal. Their concentration data were replotted (as explained previously) to provide plots of c_m/c_o vs z/r_o for several values of initial Fr and angle.

Bosanquet measured trajectories for buoyant jets discharged horizontally and at 45° to the horizontal. Fan obtained center line trajectory data for several jets discharged at various angles to uniform and stratified ambients.

Anwar, in what is probably the most complete study of this kind, measured both center line trajectory and concentration for four horizontally discharged jets with

*Since the methods of Rouse, Priestley, and Schmidt do not use the conservation of mass equation they do not have to make any assumptions concerning entrainment.

different initial Fr. In addition, center line trajectory data were given for four buoyant jets discharged at −30° to the horizontal.

These measurements show that as Fr decreases the jet begins to turn upward more rapidly. This is because the initial momentum is less significant at low Fr than at higher values. At a particular height the concentration *decreases* with increasing Froude number for horizontally discharged jets. This follows from the fact that a higher Fr jet travels a greater distance to reach a given height than does a more buoyant jet.

As the discharge angle is increased toward the vertical, the trend changes, until the jets behave much like vertically discharged jets, that is, the concentration *increases* with increasing Fr.

Abraham,[27] Bosanquet et al.,[25] Fan,[20] and Anwar[26] developed methods for the prediction of buoyant jets discharged to a quiescent medium. Abraham used the vertical and horizontal momentum equations and the concentration (energy) equations (see Fig. 3*a*):

$$\frac{d}{ds}\left(\int_0^\infty ru^2\, dr \sin\theta_2\right) = -\int_0^\infty \frac{\Delta\rho}{\rho_0} rg\, dr\,, \tag{18}$$

$$\frac{d}{ds}\left(\int_0^\infty ru^2\, dr \cos\theta_2\right) = 0\,, \tag{19}$$

$$\frac{d}{ds}\left(\int_0^\infty ru\, \Delta\rho\, dr\right) = 0\,. \tag{20}$$

Gaussian profiles were used for the density difference and velocity profiles, and b and λ were specified as empirical functions of s and θ_2. The three differential equations were then solved for u_m, $\Delta\rho_m$, and θ_2 as functions of s. x and z were determined from s and θ_2 as

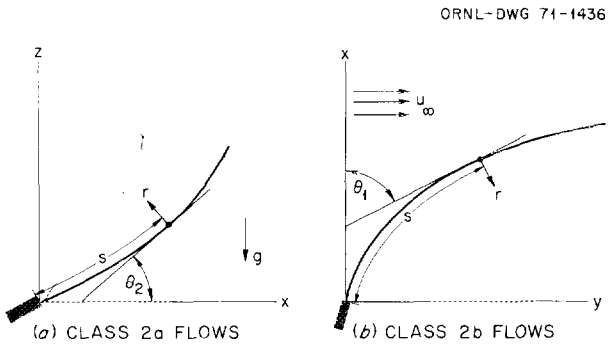

Fig. 3. Coordinate systems for class 2 jets.

$$x = \int_0^s \cos\theta_2\, ds\,,$$

$$z = \int_0^s \sin\theta_2\, ds\,. \tag{21}$$

The methods of Bosanquet, Fan, and Anwar are quite similar. They also solved Eqs. (18) to (20), but rather than specify b and λ a priori, they used the integral continuity equation (16) with $E = au_m b$. Fan suggested $a = 0.082$ using Gaussian profiles to evaluate the integrals.

2.3 Nonbuoyant Jets Discharged to a Cross Flow

Nonbuoyant jets discharged to a cross flow have been investigated experimentally by Gordier,[28] Keffer and Baines,[29] Pratte and Baines,[30] Platten and Keffer,[31] Margason,[32] and by various authors at a NASA Symposium.[33]

Gordier measured the trajectories for several jets issuing normal to a free stream with different velocity ratios $R = u_\infty/u_o$. Gordier's measurements of the center line velocity decay show that the larger R is the more rapidly the velocity decays towards the free-stream value. The total and static pressure traverses obtained by Gordier show quite clearly the characteristic horseshoe shape for a jet discharged to a cross flow.

Abramovich[10] explained that the jet cross section develops a horseshoe shape because the free stream deflects the low-speed fluid at the edge of the jet more than the fluid near the center line. This progressively deforms the shape of the cross section, as shown in Fig. 4.

Keffer and Baines also studied jets discharging normal to the free stream. Unfortunately, their measurements only cover the first 20 to $30\, r_o$ of the jet's development. Therefore, these data are less useful than are Gordier's, which extend to about $100\, r_o$. On the basis of mean flow and turbulence measurements, Keffer and Baines concluded that these jet flows display similarity, that is, the profiles at various s stations are identical when plotted with appropriate coordinates. This is an important observation since the assumption of similarity is made in all integral method analyses of such flows. Their data also show that the zone of flow establishment decreases in length with increasing R.

Platten and Keffer measured the trajectories for jets issuing at various angles to the free stream, ranging from $\theta_1 = -45$ to $+45°$. ($\theta_1 = 0$ corresponds to a jet issuing normal to the free stream; see Fig. 3*b*.) Margason also measured trajectories for jets issuing at various angles ($-90° \leqslant \theta_1 \leqslant +30°$).

Several methods exist for the prediction of nonbuoyant jets discharged to a free stream. The method of Platten and Keffer[31] is typical. They considered the integral conservation equations of mass (16), x momentum, and y momentum:

$$\frac{d}{ds}\left(\int_0^\infty u^2 r\, dr \cos\theta_1\right) = 0\,, \tag{22}$$

ORNL-DWG 71-1435

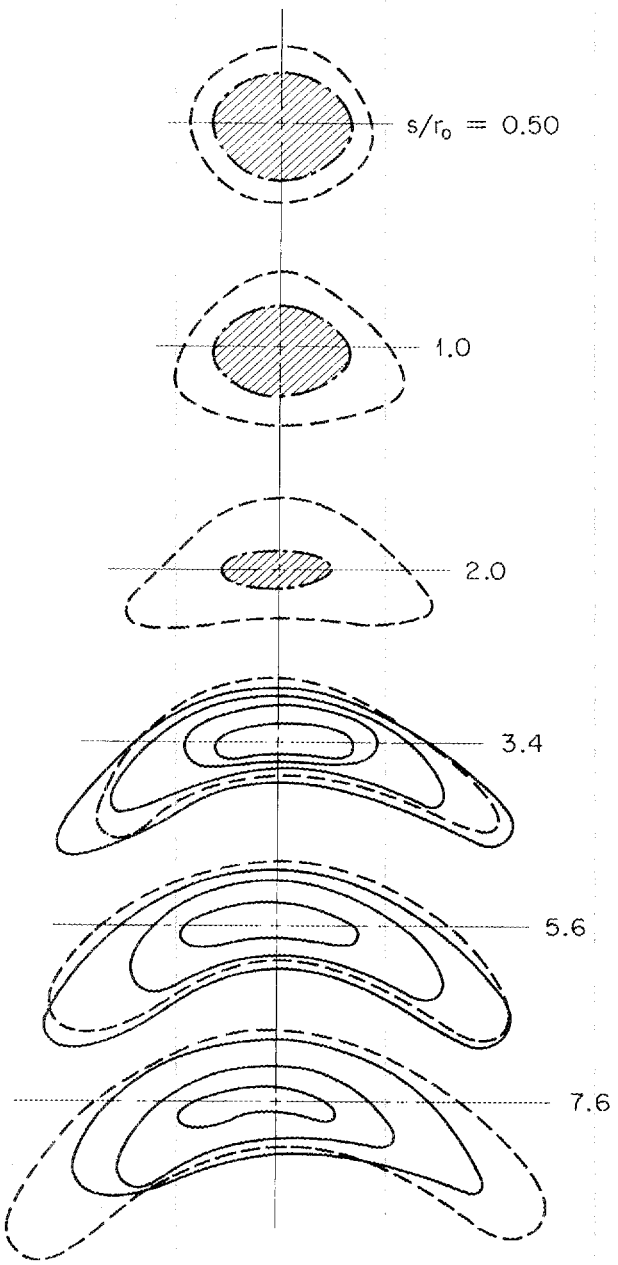

Fig. 4. Cross-sectional patterns for a nonbuoyant jet discharged to a cross flow, from Abramovich.[10]

$$\frac{d}{ds}\left(\int_0^\infty u^2 r\, dr \sin\theta_1\right) = u_\infty E\,. \tag{23}$$

Platten and Keffer used top-hat profiles and suggested, for the entrainment function:

$$E = a_1 b_{th}\,(u_{th} - u_\infty \sin\theta_1) + a_2 b_{th}\, u_\infty (\sin\theta_1 - \sin\theta_{1_0})\,. \tag{24}$$

According to them:

> The first term accounts for the entrainment due to ordinary turbulent mixing which occurs because of a difference of relative velocity. The second is an approximate function introduced to account for the vortex shear inflow.

The two legs of the horseshoe shown in Fig. 4 are the counter-rotating vortices which give rise to the second term in the entrainment function. a_1 and a_2 are the entrainment parameters, supposedly constant. Unfortunately, agreement between their theory and their experimental data could be obtained only by adjusting both constants for each particular flow; the constants ranged over a factor of about 3. Thus, one must view this method as a correlation technique rather than a predictive tool.

2.4 Buoyant Jets Discharged to a Cross Flow

Buoyant jets discharged vertically to a horizontal cross flow have been extensively studied for many years because of the interest in plume rise and dispersion from smokestacks. Briggs[34] provides an excellent review of the experimental data and methods for calculating plume rise.

The methods of Fan[20] and Hoult et al.[35,36] are studied here because they represent two of the more sophisticated plume rise theories.

Fan's method is similar to his prediction technique for buoyant jets discharged to a quiescent medium. He again solved the integral conservation equations for mass (16), energy (20), horizontal momentum, and vertical momentum:

$$\frac{d}{ds}\left(\int_0^\infty u^2 r\, dr \cos\theta_2\right) = E u_\infty + F_D \sin\theta_2\,, \tag{25}$$

$$\frac{d}{ds}\left(\int_0^\infty u^2 r\, dr \sin\theta_2\right) = -\int_0^\infty \frac{\Delta\rho}{\rho_0} r g\, dr - F_D \cos\theta_2\,. \tag{26}$$

F_D is a drag force which accounts for the variation in pressure field around the jet due to the interaction between the jet and the free stream. F_D is written in terms of a drag coefficient C_D as

$$F_D = C_D\, u_\infty^2 \sin^2 \theta_2 \sqrt{2}\, b \ . \tag{27}$$

Fan used Gaussian profiles for the velocity and density difference variations. Including the effects of the free stream changes the velocity profile:

$$u = \Delta u_m\, e^{-r^2/b^2} + u_\infty \cos \theta_2 \ , \tag{28}$$

where $\Delta u_m = u_m - u_\infty \cos \theta_2$.

Fan assumed that the entrainment rate is proportional to the vector difference between the local jet center line velocity and the free-stream velocity:

$$E = ab|\mathbf{u}_m - \mathbf{u}_\infty| = ab\,[u_\infty^{\ 2} \sin^2 \theta_2 + (\Delta u_m)^2]^{1/2} \ . \tag{29}$$

The four differential equations plus values for a and C_D permit one to compute the solution for b, Δu_m, $\Delta \rho_m$, and θ_2. The two geometrical equations (21) allow prediction of x and z.

Unfortunately, Fan found that both C_D and a must be adjusted for each particular flow. The values of a were nearly constant ($a \cong 0.4$), but the constant chosen differed significantly from the value ($a = 0.082$) which Fan used to predict the development of buoyant jets discharged to a quiescent ambient. Values for C_D ranged from 0.1 to 1.7. Thus, this method suffers from the same deficiency as does the Platten and Keffer method. The two "constants" are not constant at all!

The method of Hoult et al. used the integral conservation equations of mass (16), energy (20), streamwise momentum, and tangential momentum:

$$\frac{d}{ds}\left(\int_0^\infty u^2 r\, dr\right) = u_\infty \cos \theta_2\, E - \int_0^\infty \frac{\Delta\rho}{\rho_0} rg\, dr \sin \theta_2 \ , \tag{30}$$

$$\frac{d\theta_2}{ds}\left(\int_0^\infty u^2 r\, dr\right) = -\, u_\infty \sin \theta_2\, E - \int_0^\infty \frac{\Delta\rho}{\rho_0} rg\, dr \cos \theta_2 \ . \tag{31}$$

Note that the momentum equations used by Hoult do not contain the drag force terms included by Fan. (However, aside from the F_D terms, the two sets of momentum equations are equivalent.) Hoult et al. used top-hat profiles and the following entrainment function:

$$E = a_1 b_{th} |u_{th} - u_\infty \cos \theta_2| + a_2 b_{th}\, u_\infty \sin \theta_2 \ . \tag{32}$$

According to them:

> There are basically two entrainment mechanisms: one is due to the difference between the plume velocity and wind velocity component parallel to the plume and the other to the wind velocity component normal to the plume.

The two entrainment coefficients were assumed constant. However, the values suggested are somewhat different in the two references cited; $a_1 = 0.12$ and a_2 ranges from 0.6 to 0.9. In a more recent report,[37] the values selected are $a_1 = 0.11$ and $a_2 = 0.60$.

Even though the methods of Fan and Hoult use the same basic differential equations they differ substantially in their entrainment function and in the use of drag force terms. Hoult et al. eschew the F_D terms because they feel that the drag force is important only in the first few nozzle diameters downstream of the outfall. Both methods contain two adjustable constants.

Extensive field measurements of power plant plumes have been conducted by Thomas et al.[38,39] at several Tennessee Valley Authority plants. Bringfelt[40] made similar measurements at industrial chimneys in Sweden.

Laboratory experiments on buoyant jets discharged to a cross flow were performed by Fan[20] and Hewett et al.[41] Fan measured plume trajectories and center line concentrations at four different Fr and four different R. His experiments were conducted in a water tank with a uniform free stream of homogeneous density.

Hewett, working with a wind tunnel, measured plume trajectories and center line temperature decay for very low Fr plumes discharged to stratified flowing ambients.

2.5 Summary

There exists a large body of experimental data for class 1 and class 2 jet flows. However, with the exception of the simple momentum jet and the simple plume very few velocity and density profiles normal to the jet axis have been measured. Turbulence measurements are even more scanty.

For most of the class 1 flows both the center line velocity and density difference (or equivalent scalar property) have been measured. Unfortunately, this has been the exception rather than the rule for class 2

flows. The flows of Anwar, Fan, and Hewett are notable exceptions.

Data for class 3 flows are completely nonexistent. Thus, there are several gaps in our experimental knowledge concerning these free turbulent shear flows.

Several theoretical methods exist for the prediction of class 1 and class 2 flows. These methods are based on the integral conservation equations, derived by considering a control volume infinitesimally thick in the streamwise direction and of finite extent normal to the jet axis. The velocity and density difference profiles are assumed to be similar. The methods either use the continuity equation in which case the entrainment function must be specified or they use the mechanical energy integral equation for which the turbulent shear stress integral must be specified. With the exception of a prototype method developed by Telford,[42] no methods make explicit mention of the turbulence.

The purposes of the work described in the following chapters are to: (1) derive the basic partial differential equations for a class 3 jet; (2) develop an integral method based on these equations; and (3) use this method to predict the physical effects of thermal discharges from power plants. The integral equations developed from these basic partial differential equations contain terms which do not appear in previous integral methods. A generalized entrainment function is formulated, based on the work of Fox[19] and Hoult,[35] which adequately predicts class 1 and class 2 jets and should also provide reasonable predictions for class 3 flows.

3. DERIVATION OF THE INTEGRAL EQUATIONS

3.1 The Basic Equations

The problem considered here involves the dynamics of a buoyant jet discharged from a round diffuser or pipe. The jet density may differ from the ambient density because of temperature and/or salinity differences. The motion of the jet is determined by: the initial conditions at the diffuser exit (velocity, buoyancy, outlet orientation, diffuser radius), the buoyancy force, and the ambient velocity, turbulence levels, and density stratification.

The basic equations governing the dynamics of the jet as it moves through the ambient are:

1. conservation of mass,
2. conservation of energy,
3. conservation of salt (or other scalar component),
4. conservation of momentum (three scalar equations).

These six equations are sufficient to solve for the pressure, three velocity components, temperature, and salinity. These equations, written in general vector form, are:[43,44]

$$\frac{\partial \rho}{\partial \tau} + \nabla\cdot(\rho \mathbf{v}) = 0 , \tag{33}$$

$$\frac{\partial t}{\partial \tau} + \mathbf{v}\cdot(\nabla t) = \frac{1}{\rho c_v} \nabla\cdot(k \nabla t) + \frac{\nu}{c_v} \Phi - t\left(\frac{\partial p}{\partial t}\right)_\rho (\nabla\cdot\mathbf{v}) , \tag{34}$$

$$\frac{\partial c}{\partial \tau} + \mathbf{v}\cdot(\nabla c) = \nabla\cdot(D \nabla c) , \tag{35}$$

$$\frac{\partial \mathbf{v}}{\partial \tau} + \frac{1}{2}\nabla \mathbf{v}^2 - \mathbf{v} \times (\nabla \times \mathbf{v}) = \frac{-\nabla p + \rho \mathbf{F}}{\rho} + \nu \nabla^2 \mathbf{v}. \tag{36}$$

For our problem, the following simplifying assumptions can be made:

1. steady flow, in the mean,
2. fully turbulent flow; molecular diffusion is neglected,
3. incompressible flow; the density variation appears only in the buoyancy term (Boussinesq approximation) of the momentum equation,
4. constant fluid properties,
5. small Eckert number (flow velocity); frictional heating is neglected in the energy equation.

With these assumptions Eqs. (33) through (36) become:

$$\nabla\cdot\mathbf{v} = 0 , \tag{37}$$

$$\mathbf{v}\cdot(\nabla t) = 0 , \tag{38}$$

$$\mathbf{v}\cdot(\nabla c) = 0 , \tag{39}$$

$$\frac{1}{2}\nabla \mathbf{v}^2 - \mathbf{v} \times (\nabla \times \mathbf{v}) = \frac{-\nabla p + \rho \mathbf{F}}{\rho_0} . \tag{40}$$

The pressure gradient term in Eq. (40) can be written as

$$\nabla p = \rho_\infty \mathbf{g} + \nabla p^* ,$$

where $\rho_\infty \mathbf{g}$ is the hydrostatic pressure gradient, due solely to the weight of the ambient fluid, and ∇p^* is the difference between the local and hydrostatic pressure gradients.

The body force term in Eq. (40) is due to the weight of the jet fluid, that is,

$$\rho \mathbf{F} = \rho \mathbf{g} .$$

Combining the above two expressions yields

$$-\nabla p + \rho \mathbf{F} = (\rho - \rho_\infty)\,\mathbf{g} - \nabla p^* . \tag{41}$$

An equation of state for ρ can be derived by expanding $\rho(t, c)$ in a double Taylor series about the reference density ρ_0:

$$\rho = \rho_0\,[1 - \beta(t - t_0) - \gamma(c - c_0)] , \tag{42}$$

where

$$\beta = -\frac{1}{\rho_0}\left(\frac{\partial \rho}{\partial t}\right)_p ,$$

$$\gamma = -\frac{1}{\rho_0}\left(\frac{\partial \rho}{\partial c}\right)_t .$$

Then

$$\frac{\rho - \rho_\infty}{\rho_0} = \beta(t_\infty - t) + \gamma(c_\infty - c) . \tag{43}$$

This equation of state (43) is used to determine the local density from a solution to Eqs. (38) and (39).

With Eq. (41), the momentum equation (40) becomes

$$\frac{1}{2}\nabla \mathbf{v}^2 - \mathbf{v} \times (\nabla \times \mathbf{v}) = \frac{\rho - \rho_\infty}{\rho_0}\,\mathbf{g} - \frac{1}{\rho_0}\,\nabla p^* . \tag{44}$$

In order to solve Eqs. (37) to (39) and (44) an appropriate coordinate system must be defined in which to express these equations.

In general, the jet center line will follow a three-dimensional trajectory because the jet momentum vector, buoyancy force, and cross-flow vector may all point in different directions. The most suitable coordinate system for this kind of problem is a "natural" system which moves with the jet center line. Figure 5 shows the coordinate system used in this analysis. The system is fully described in Appendix A.

In Appendix B the governing equations (37) to (39) and (44) are written in terms of this new coordinate system. The result is a set of six nonlinear coupled partial differential equations with three independent variables — s, r, ϕ. Because these equations are immensely difficult to solve we shall make certain

ORNL-DWG 71-1434

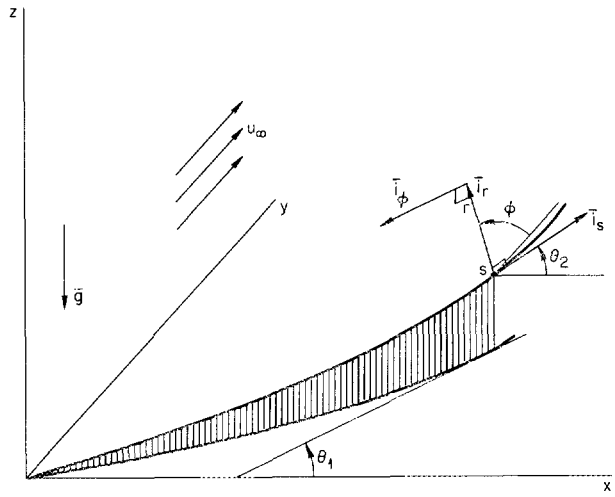

Fig. 5. Natural coordinate system for buoyant jet analysis.

physically reasonable assumptions which will allow us to obtain solutions.

We first assume the flow to be axisymmetric, that is, $w = 0$, $\partial/\partial\phi = 0$. For simple momentum jets and buoyant jets discharged vertically up into a quiescent ambient, the motion is indeed axisymmetric. For more general cases the flow may not be axisymmetric. In particular, for jets in a cross flow the fluid tends to roll up into two counterrotating parallel vortices;[10,28] see Fig. 4. In spite of this evidence we shall see (in Chap. 4) that reasonable predictions can be obtained with this assumption. The asymmetry can probably be ignored because the governing equations are (later in this chapter) integrated over the jet's cross section, and this effectively averages out the asymmetry. We shall also neglect the nonhydrostatic pressure gradient.

These axisymmetric equations are derived in Appendix C. First, the complete momentum equations are written in the s (parallel to the jet axis), z (parallel to the buoyancy force), and y (parallel to the free-stream) directions. Then, these equations and the continuity, energy, and concentration equations are integrated with respect to ϕ to yield another set of six differential equations. However, this new set of equations contains only s and r as independent variables.

Since these equations do not explicitly include the effects of turbulence, they are rewritten in terms of average and fluctuating components.

The flow in a buoyant turbulent jet is of the boundary layer type; that is, gradients in the streamwise (s) direction are much smaller than are gradients in the normal (r) direction and $\bar{u} \gg \bar{v}$. Invoking the usual

boundary layer approximations[4,5] simplifies the equations considerably.

These equations, (C-17) to (C-22), while considerably simpler than those of Appendix B, are still not easy to solve. Several groups (particularly at the Los Alamos Scientific Laboratory and the National Center for Atmospheric Research) have developed computer techniques for solving similar fluid mechanics problems. However, the solutions require large investments in computer time and programming effort. Therefore, we have elected to reduce the complexity of these equations by one more order.

3.2 Integral Equations

Equations (C-17) to (C-22) are formally integrated in the radial direction from the jet axis to infinity. The resulting set of ordinary differential equations contains s as the single independent variable.

Derivation of these "integral" equations involves no new assumptions. However, the process of integration, which implies an average, wipes out some of the information content of the partial differential equations. This missing information is implicitly reintroduced by the entrainment function and velocity, temperature, and concentration profiles which must be specified in order to achieve closure.

The final equations are:

continuity equation:

$$\frac{d}{ds}\left(\int_0^\infty \bar{u} r\, dr\right) = -\lim_{r\to\infty}\left(r\bar{v}\right) = E\,, \tag{45}$$

energy equation:

$$\frac{d}{ds}\left[\int_0^\infty \bar{u}\left(\bar{t}-t_\infty\right) r\, dr\right] = -\frac{dt_\infty}{ds}\int_0^\infty \bar{u} r\, dr - \lim_{r\to\infty}\left(r\overline{v't'}\right), \tag{46}$$

concentration equation:

$$\frac{d}{ds}\left[\int_0^\infty \bar{u}\left(\bar{c}-c_\infty\right) r\, dr\right] = -\frac{dc_\infty}{ds}\int_0^\infty \bar{u} r\, dr - \lim_{r\to\infty}\left(r\overline{v'c'}\right), \tag{47}$$

s momentum equation:

$$\frac{d}{ds}\left(\int_0^\infty \bar{u}^2\, r\, dr\right) = \int_0^\infty \frac{\rho_\infty - \bar{\rho}}{\rho_0} r\, dr\, g S_2 + Eu_\infty S_1\, C_2 - \lim_{r\to\infty}\left(r\overline{u'v'}\right), \tag{48}$$

k momentum equation:

$$\frac{d}{ds}\left(\int_0^\infty \bar{u}^2 r\, dr\right) S_2 = \int_0^\infty \frac{\rho_\infty - \bar{\rho}}{\rho_0} r\, dr\, g - \lim_{r\to\infty}\left(r\overline{u'v'}\right) S_2 - q\,\frac{C_2}{\rho_2}\,, \tag{49}$$

j momentum equation:

$$\frac{d}{ds}\left(\int_0^\infty \bar{u}^2 r\, dr\right) S_1\, C_2 = Eu_\infty - \lim_{r\to\infty}\left(r\overline{u'v'}\right) S_1\, C_2 - q\left(\frac{C_1\, C_2}{\rho_1} - \frac{S_1\, S_2}{\rho_2}\right), \tag{50}$$

i momentum equation:*

$$\frac{d}{ds}\left(\int_0^\infty \bar{u}^2 r\, dr\right) C_1\, C_2 = q\left(\frac{S_1\, C_2}{\rho_1} + \frac{C_1\, S_2}{\rho_2}\right) - \lim_{r\to\infty}\left(r\overline{u'v'}\right) C_1\, C_2\,, \tag{51}$$

where

$$q = \int_0^\infty \bar{u}^2 r\, dr - \frac{1}{4}E^2 - \frac{1}{4}\lim_{r\to\infty}\left(r^2\overline{v'^2}\right).$$

Equations (49) and (50) can be simplified by using Eq. (48). The reduced equations are

$$\frac{d\theta_1}{ds} = \frac{Eu_\infty C_1}{qC_2}\,, \tag{52}$$

$$\frac{d\theta_2}{ds} = \frac{\int_0^\infty [(\rho_\infty - \bar{\rho})/\rho_0]\, r\, dr\, g C_2 - Eu_\infty S_1\, S_2}{q}. \tag{53}$$

These equations contain several terms which do not appear in the equations used by other investigators. Some of the new terms involve the ambient turbulence, for example, $\lim_{r\to\infty}(r\overline{u'v'})$, and others appear in q (the last two terms in q). The turbulence terms are zero for jets discharged to nonturbulent ambients, and the additional terms in q are important only for jets discharged to a cross flow in the region near the origin where the curvature is large.

Equations (45) to (48), (52), and (53) form the basis for the integral method developed in the next chapter. The boundary conditions for these equations specify values for the integrals on the left-hand sides of Eqs. (45) to (48) and θ_1 and θ_2 at $s = 0$.

*The i momentum equation is included here only for completeness. It can be derived from the other three momentum equations; that is, the four momentum equations are linearly dependent.

The Cartesian coordinates (x, y, z) of the center line can be expressed in terms of s, θ_1, and θ_2 as follows:

$$x = \int_0^s C_1 \, C_2 \, ds \, ,$$

$$y = \int_0^s S_1 \, C_2 \, ds \, ,$$

$$z = \int_0^s S_2 \, ds \, . \qquad (54) \, .$$

These geometrical constraints are analogous to Eqs. (21) developed for a class 2 flow.

Equation (45) is a statement of the conservation of mass. The rate of change in mass flux through any cross section of the jet must be equal to the influx from outside the jet, that is, the entrainment. The entrainment, E, is a strong function of the turbulence levels within the jet. However, in most integral method solutions (including this one) the turbulence is not explicitly considered. So the entrainment function is assumed to depend on mean flow quantities. The development of an accurate and general entrainment function is a difficult but essential task. This is discussed in Chap. 4.

Equations (46) and (47) are statements of the conservation of energy (temperature) and conservation of salt (concentration). The conservation equation for any scalar quantity is identical to these equations. The rate of change of flux of a scalar past a cross section of the jet is equal to the inflow (with the entrained fluid) of the ambient concentration of the scalar and the inflow due to turbulence at the edge of the jet.

Equation (48) is a momentum balance in a direction parallel to the local jet axis. The flux of momentum through the cross section is equal to the buoyancy force on that section and the circumferential momentum inflow due to entrainment and the ambient Reynolds stresses.

Equation (52) shows how changes in θ_1 depend on the orientation of the jet and the free-stream velocity, u_∞. The cross flow tends to turn the jet in the y direction. This turning effect is most pronounced when the jet is perpendicular to the free stream. Note that for $\theta_2 \cong 90°$ Eq. (52) implies that $d\theta_1/ds$ is infinite. This is a reflection of the fact that, for θ_2 near 90°, θ_1 is undefined. When θ_2 is close to 90°, Eq. (52) is not used.

Equation (53) shows how changes in θ_2 depend on the buoyancy force and the free stream. The influence of buoyancy is greatest when the jet is horizontal and decreases as the jet approaches the vertical.

3.3 Summary

In this chapter and the Appendices the basic differential equations governing the development of a momentum jet have been derived in a new, natural coordinate system which moves with the jet center line. The resulting equations and boundary conditions are extremely complicated.

Therefore, the equations have been simplified by assuming the flow to be axisymmetric and then integrating the governing equations over a cross section of the jet (perpendicular to $\mathbf{i}_s$). The final ordinary differential equations (45) to (50) form the basis for the integral method solution developed in the next chapter. The assumptions implicit in the derivation of these integral equations are restated:

1. the flow is steady, in the mean,
2. the flow is fully turbulent; molecular diffusion is neglected,
3. the fluid is assumed incompressible; density variations are included only in the buoyancy terms,
4. all other fluid properties are assumed constant,
5. fluid velocities are assumed low enough so that frictional heating can be neglected,
6. the pressure variation is assumed to be purely hydrostatic,
7. changes in density are assumed to be small enough so that the linear equation of state (43) is valid,
8. the flow within the jet is assumed to be axisymmetric,
9. the flow within the jet is assumed to be of boundary layer type and the boundary layer approximations are valid,
10. the jet is discharged to an ambient fluid of infinite extent.

4. INTEGRAL METHOD SOLUTION

4.1 Velocity and Density Difference Profiles

The ordinary differential equations (45) to (48), (52), and (53) and the algebraic equation of state (43) form the basis for the integral method solution developed here. For the remainder of this report the free-stream turbulence terms in all equations are neglected because laboratory data showing the influence of ambient turbulence levels on jet development are nonexistent. In order to solve this system of equations, the velocity, temperature, concentration, and density profiles normal

to the jet axis must be specified. Existing integral methods assume that these profiles are similar, that is, the shape of the profile (when plotted in appropriate coordinates) is invariant with s, the streamwise coordinate. The two most popular profile shapes are the Gaussian and the top-hat, shown in Fig. 2.

For class 3 flows the Gaussian velocity and density (temperature and concentration) difference profiles are

$$\bar{u} = \Delta u_m \, e^{-r^2/b^2} + u_{12} \, ,$$

$$\bar{\rho} - \rho_\infty = \Delta\rho_m \, e^{-(r/\lambda b)^2} \, , \tag{55}$$

where

$$\Delta u_m = u_m - u_{12} \, .$$

The corresponding top-hat profiles are

$$\bar{u} = u_{th}, r \leqslant b_{th} \, ,$$

$$= 0, r > b_{th} \, ,$$

$$\bar{\rho} - \rho_\infty = \Delta\rho_{th}, r \leqslant \lambda_{th} b_{th} \, ,$$

$$= 0, r > \lambda_{th} b_{th} \, , \tag{56}$$

where $\Delta\rho_{th}$ and u_{th} are the "average" density difference and velocity at any s station and b_{th} is a characteristic jet width.

Theoretical predictions using either set of profiles are identical, provided that Eqs. (13) and (14) are observed. Equating the integral mass flux, momentum flux, and energy flux yields the following relations between the top-hat parameters and the Gaussian parameters:

$$u_{th} = \frac{1}{2}(u_m + u_{12}) \, ,$$

$$b_{th} = \sqrt{2}\, b \, ,$$

$$\Delta\rho_{th} = \frac{\lambda^2}{\lambda^2+1} \Delta\rho_m \, . \tag{57}$$

The predictions provided by this new method will ultimately be used to help assess the ecological consequences of thermal discharges from power plants. Here the interest is in the center line temperature and temperature field, as well as the jet trajectory. Hence, for our purposes it is algebraically easier to use the Gaussian profiles.

Using the Gaussian profiles of Eq. (55) in Eqs. (45) to (48), (52), and (53) yields the following system of ordinary differential equations:*

$$\frac{d}{ds}\left(\frac{\mathrm{v}^* b^2}{2}\right) = E \, , \tag{58}$$

$$\frac{d}{ds}\left[\frac{\Delta t_m \, b^2 \lambda^2}{2}\left(u_{12} + \frac{\Delta u_m}{\lambda^2+1}\right)\right] = -\frac{dt_\infty}{ds}\left(\frac{\mathrm{v}^* b^2}{2}\right) \, , \tag{59}$$

$$\frac{d}{ds}\left[\frac{\Delta c_m \, b^2 \lambda^2}{2}\left(u_{12} + \frac{\Delta u_m}{\lambda^2+1}\right)\right] = -\frac{dc_\infty}{ds}\left(\frac{\mathrm{v}^* b^2}{2}\right) \, , \tag{60}$$

$$\frac{d}{ds}\left(\frac{\mathrm{v}^{*2} \, b^2}{4}\right) = E u_{12} - \frac{\Delta\rho_m}{\rho_o}\frac{b^2}{2}\lambda^2 g S_2 \, , \tag{61}$$

$$\frac{d\theta_1}{ds} = \frac{E u_\infty C_1}{q C_2} \, , \tag{62}$$

$$\frac{d\theta_2}{ds} = \frac{-(\Delta\rho_m/\rho_o)(b^2/2)\lambda^2 g C_2 - E u_\infty S_1 S_2}{q} \, , \tag{63}$$

where

$$\mathrm{v}^* = u_m + u_{12} \, ,$$

$$q = \frac{1}{4}(b^2 \, \mathrm{v}^{*2} - E^2) \, .$$

The solution to these six equations yields values of u_m, t_m, c_m, b, θ_1, and θ_2 as functions of s. Equations (54) give x, y, and z in terms of s, θ_1, and θ_2.

These integral equations can be nondimensionalized by normalizing all the variables on the jet properties at the diffuser outlet, that is, u_o, r_o, t_o, c_o, and ρ_o. Writing the equations in this form introduces three nondimensional parameters, R, Fr, and T. R indicates the importance of the free-stream velocity relative to the initial jet velocity, Fr is a measure of the relative importance of the buoyancy and inertia forces, and T is the stratification parameter and indicates the importance of the ambient density variation.

---

*$\sqrt{2}\, b$ is taken to be the outer edge of the jet for the integrals involving u_{12}; for example,

$$\int_0^\infty u r \, dr \cong \int_0^\infty \Delta u_m e^{-r^2/b^2} \, r \, dr + \int_0^{\sqrt{2}b} u_{12} \, r \, dr \, .$$

4.2 Generalized Entrainment Functions

In order to achieve closure in Eqs. (58) to (63), an entrainment function must be specified for the right-hand side of Eq. (58). The entrainment is a key determinant of the growth and development of buoyant jets.

The entrainment (ingestion) of free-stream fluid is largely determined by the turbulence structure inside the jet, particularly near the edge. The edge of a free shear flow is a highly irregular time-dependent surface which separates the jet from the free-stream fluid. This irregularity is clearly shown by intermittency measurements which indicate the fraction of time that the fluid flowing past a certain point is turbulent. The intermittency decreases from 1.0 at the jet center to 0.0 for large radii. Corrsin and Kistler[46] suggest that the entrainment of free-stream fluid takes place across a thin "superlayer" at the edge of the turbulent jet.

Unfortunately, ignorance concerning the turbulence structure makes it difficult to develop a suitable entrainment function based on the turbulence structure of buoyant jets. Therefore, it has been common practice to formulate entrainment equations using the mean flow variables (u_m, u_{12}, $\Delta\rho_m$, b).

The entrainment function should depend on the following factors:

1. local mean flow conditions within the jet, u_m and b,
2. local buoyancy within the jet, Fr_L,
3. velocity ratio, R,
4. initial jet orientation, θ_{1o} and θ_{2o},
5. ambient turbulence.*

The entrainment function used by Morton et al.[23] and Fan,[20] $E = au_m b$, for the prediction of buoyant jets discharged to a quiescent medium includes only the local mean flow conditions; that is, the influence of conditions 2 to 4 is neglected.

The entrainment function derived by Fox[19] for vertically discharged buoyant jets to a quiescent medium,

$$E = (a_1 + a_2/\mathrm{Fr}_L)\, u_m b \ ,$$

includes conditions 1 and 2, an improvement over Morton's entrainment hypothesis.

*The effect of ambient turbulence on entrainment is not considered here, again because of the lack of pertinent data.

Platten and Keffer's[31] function, developed for non-buoyant jets discharged to a cross flow,*

$$E = a_1 b|\, u_m - u_{12}| + a_2 b u_\infty (S_1 C_2 - S_{1_0} C_{2_0}) \ , \quad (64)$$

includes conditions 1, 3, and 4. Hoult's[35] entrainment function, developed for buoyant jets discharged to a cross flow,

$$E = a_1 b|u_m - u_{12}| + a_2 b u_\infty \sqrt{1-(S_1 C_2)^2} \ , \quad (65)$$

also includes conditions 1, 3, and 4.

Our study of existing prediction methods reveals that no single entrainment function accounts for all the factors believed to be important.

The method used by Fox[19] to derive an entrainment function for vertically discharged buoyant jets can be applied to more general flows. The mechanical energy integral equation is derived by multiplying the streamwise momentum equation (C-20) by $\bar{u}$ and integrating across the jet. The resulting equation is:

$$\frac{d}{ds}\left(\int_0^\infty \bar{u}^3\, r\, dr\right) = 2\int_0^\infty \frac{\rho_\infty - \bar{\rho}}{\rho_0}\bar{u} r\, dr\, g S_2 + E u_{12}^{\ 2} - 2\int_0^\infty \bar{u}\, \frac{\partial(r\overline{u'v'})}{\partial r}\, dr \ . \quad (66)$$

The shear stress integral in Eq. (66) is assumed to be similar so that it scales as (for jets discharged to a quiescent medium):

$$\int_0^\infty \bar{u}\, \frac{\partial(r\overline{u'v'})}{\partial r}\, dr = I\, u_m^{\ 3} b \ , \quad (67)$$

where I is the similarity integral.

Substitution of the Gaussian profiles and Eq. (67) into Eq. (66) yields, for $R = 0$,

$$\frac{d}{ds}\left(\frac{u_m^{\ 3} b^2}{6}\right) = \frac{-\Delta\rho_m}{\rho_0} u_m b^2 g S_2 \frac{\lambda^2}{\lambda^2 + 1} - 2I u_m^{\ 3} b \ . \quad (68)$$

It can be shown that

$$u_m^{\ 2} \frac{d}{ds}(u_m b^2) = 2u_m \frac{d}{ds}(u_m^{\ 2} b^2) - \frac{d}{ds}(u_m^{\ 3} b^2) \ . \quad (69)$$

*To facilitate comparisons the entrainment functions discussed here have been generalized for class 3 flows and converted to Gaussian form.

Substituting Eq. (58) into the left-hand side of Eq. (69) and Eqs. (61) and (68) into the right-hand side of (69) yields an expression for the entrainment function, for flows with $R = 0$,

$$E = \left(a_1 + \frac{a_2}{Fr_L} S_2\right) u_m b \ , \tag{70}$$

where

$$a_1 = 6I$$

and

$$a_2 = 2\lambda^2 - \frac{3\lambda^2}{\lambda^2 + 1} \ .$$

$a_1 u_m b$ represents the entrainment due to the internal jet turbulence. a_1 is the entrainment coefficient in Morton's[23] or Fan's[20] entrainment function, $E = a_1 u_m b$. Experimental data[3] indicate that, for non-buoyant jets,

$$a_1 = 0.057 \ .$$

The second term in this new entrainment function, $a_2 S_2 u_m b/\mathrm{Fr}_L$, represents the incremental entrainment due to the buoyancy force. For large Froude numbers this term is negligible, but for small Froude numbers it can be significant. With $\lambda = 1.11$ (large Fr), $a_2 = 0.81$; with $\lambda = 1.16$ (small Fr), $a_2 = 0.97$. Since this second term is significant only for low Froude numbers it seems reasonable to fix a_2 as

$$a_2 = 0.97 \ . \tag{71}$$

This new entrainment function satisfies three of the five necessary conditions listed previously. Attempts to derive an entrainment function, using this method, for jets discharged to a cross flow ($R \neq 0$) failed to yield reasonable results, probably because the assumption of similar shear stress profiles is quite incorrect for $R \neq 0$.

However, the new entrainment function (70) can be combined with either Eq. (64) or Eq. (65) to provide a generalized entrainment function which satisfies all four conditions.

Thus, a combination of Eq. (70) and the Hoult function yields

$$E = \left(a_1 + \frac{a_2}{\mathrm{Fr}_L} S_2\right) b|u_m - u_{12}| + \left(a_3 + \frac{a_4}{\mathrm{Fr}_L} S_2\right) u_\infty b\sqrt{1 - (S_1 C_2)^2} \ . \tag{72}$$

Similarly, combining Eq. (70) and the Platten and Keffer function yields

$$E = \left(a_1 + \frac{a_2}{\mathrm{Fr}_L} S_2\right) b|u_m - u_{12}| + \left(a_3 + \frac{a_4}{\mathrm{Fr}_L} S_2\right) u_\infty b(S_1 C_2 - S_{1_0} C_{2_0}) \ . \tag{73}$$

These two entrainment functions, both of which contain four coefficients, appear to satisfy the conditions listed earlier. The method used to systematically determine these constants is explained in the next section, where values for the a_i are given.

4.3 Comparison with Experiments

One could adjust the four constants in Eq. (72) or (73) in such a way that the predictions are, in some sense, optimized. This "optimization" process is highly subjective and dependent on the optimizer's thoughts concerning the relative importance of different flows. Certainly this procedure is not unique; that is, different people would produce different sets of entrainment coefficients a_i.

On the other hand, one can define these constants using experimental data from specialized flows, which is the method used here. For example, the only term appearing in the entrainment function for the simple momentum jet is the first (a_1) term. From the discussion in Chap. 2, we know that $a_1 = 0.057$, so a_1 is fixed at this value for all flows. Similarly, the discussion earlier in this chapter indicates that $a_2 = 0.97$ from low Froude number data, so a_2 is fixed at this value for all flows.

We also assume that the ratio of buoyancy-induced entrainment to internal-turbulence-induced entrainment is the same for both terms in the entrainment function. This implies that $a_4/a_3 = a_2/a_1$, which reduces Eqs. (72) and (73) to

$$E = \left(a_1 + \frac{a_2}{\mathrm{Fr}_L} S_2\right) [b|u_m - u_{12}| + a_5 u_\infty b\sqrt{1 - (S_1 C_2)^2}] \ , \tag{74}$$

$$E = \left(a_1 + \frac{a_2}{\mathrm{Fr}_L} S_2\right) [b|u_m - u_{12}| + a_5 u_\infty b(S_1 C_2 - S_{1_0} C_{2_0})] \ . \tag{75}$$

Then, only one constant, a_5, must be empirically determined.

At this point, the entrainment function for jets discharged to a quiescent or coflowing ambient is completely determined. Furthermore, the two entrainment equations (74) and (75) are identical for these flows:

$$E = \left(0.057 + \frac{0.97}{\mathrm{Fr}_L} S_2\right) b|u_m - u_{12}| \,. \qquad (76)$$

Therefore, we can now compare experimental data with theoretical predictions for these flows since the predictions are independent of a_5. Figures 6–18 illustrate the quality of prediction* obtained with the integral equations (58) to (63) and the entrainment function (76) with a_1 and a_2 fixed a priori. Theory and data are compared for 71 flows of this type; the values of Fr, R, θ_1, θ_2, and T for these flows are presented in Table 1.

*These predictions are computed using an IBM 360/75 computer and Hamming's modified predictor-corrector method (IBM Scientific Subroutine Package: HPCG) for solution of the differential equations. The initial conditions, at the beginning of the zone of established flow, are derived in Appendex D.

Table 1. Experimental jet flows studied

ID No.	Ref.	Class	Fig.	Fr	R	θ_1	θ_2	T
1101	3,5,6,10	1a	6	∞	0	0°	0°	∞
1201	8	1b	7,8	∞	0.25	90	0	∞
1203	8	1b	7,8	∞	0.46	90	0	∞
1204	8	1b	7,8	∞	0.50	90	0	∞
3511	18	1c	9	109	0	0	90	83.4
3512	18	1c	9	303	0	0	90	57.0
3513	18	1c	9	534	0	0	90	77.1
3514	18	1c	9	101	0	0	90	141
3515	18	1c	9	138	0	0	90	93.6
3516	18	1c	9	360	0	0	90	92.4
3517	18	1c	9	445	0	0	90	67.6
3518	18	1c	9	506	0	0	90	92.1
3519	18	1c	9	121	0	0	90	134
3521	20	1c	9	2450	0	0	90	87.5
3522	20	1c	9	5618	0	0	90	339
3523	20	1c	9	648	0	0	90	205
3531	19	1c	9	86500	0	0	90	2123
3532	19	1c	9	8450	0	0	90	2062
3533	19	1c	9	139000	0	0	90	2020
3534	19	1c	9	182000	0	0	90	885
3535	19	1c	9	188000	0	0	90	893
3536	19	1c	9	154000	0	0	90	168
3537	19	1c	9	46200	0	0	90	150
3538	19	1c	9	2590	0	0	90	885
3539	19	1c	9	11550	0	0	90	282
3541	17	1c	9	20.6	0	0	90	527
3542	17	1c	9	19.0	0	0	90	896
3543	17	1c	9	17.0	0	0	90	694
3544	17	1c	9	16.8	0	0	90	1236
3545	17	1c	9	14.4	0	0	90	908
3546	17	1c	9	13.2	0	0	90	1416
3548	17	1c	9	12.6	0	0	90	1586
3550	17	1c	9	12.6	0	0	90	1825
3551	17	1c	9	12.6	0	0	90	1667
3552	17	1c	9	11.5	0	0	90	2038
3553	17	1c	9	11.2	0	0	90	2118
3555	17	1c	9	10.8	0	0	90	2587
3556	17	1c	9	10.6	0	0	90	2918
3557	17	1c	9	10.5	0	0	90	3222
3558	17	1c	9	10.6	0	0	90	3685
3559	17	1c	9	11.0	0	0	90	4968
3560	17	1c	9	11.8	0	0	90	4884
3561	17	1c	9	11.8	0	0	90	6287
3563	17	1c	9	13.3	0	0	90	7845

Table 1 (continued)

ID No.	Ref.	Class	Fig.	Fr	R	θ_1	θ_2	T
3001	20	2a	10	8712	0	0	0	∞
3002	20	2a	10	33800	0	0	0	∞
3003	20	2a	10	3578	0	0	0	∞
3004	20	2a	11	2178	0	0	0	∞
3006	20	2a	11	416	0	0	0	∞
3251	26	2a	12,13	32.0	0	0	0	∞
3252	26	2a	12,13	72.0	0	0	0	∞
3253	26	2a	12,13	128.0	0	0	0	∞
3254	26	2a	12,13	242.0	0	0	0	∞
3101	15	2a	14	50.0	0	0	0	∞
3102	15	2a	14	200	0	0	0	∞
3103	15	2a	14	450	0	0	0	∞
3104	15	2a	14	800	0	0	0	∞
3109	15	2a	15	50.0	0	0	30	∞
3110	15	2a	15	200	0	0	30	∞
3111	15	2a	15	450	0	0	30	∞
3112	15	2a	15	800	0	0	30	∞
3117	15	2a	16	50.0	0	0	90	∞
3118	15	2a	16	200	0	0	90	∞
3119	15	2a	16	450	0	0	90	∞
3120	15	2a	16	800	0	0	90	∞
3501	20	2a	17	1352	0	0	0	2454
3502	20	2a	17	3200	0	0	0	10997
3505	20	2a	17	7200	0	0	0	1030
3507	20	2a	18	338	0	0	2.8	227
3508	20	2a	18	800	0	0	39.1	214
3509	20	2a	18	2601	0	0	45	423
2004	31	2b	19	∞	0.25	−45	0	∞
2006	31	2b	19	∞	0.25	−15	0	∞
2008	31	2b	19	∞	0.25	15	0	∞
2010	31	2b	20	∞	0.167	−45	0	∞
2012	31	2b	20	∞	0.167	−15	0	∞
2014	31	2b	20	∞	0.167	15	0	∞
2016	31	2b	20	∞	0.167	45	0	∞
2017	31	2b	21	∞	0.125	−45	0	∞
2019	31	2b	21	∞	0.125	−15	0	∞
2021	31	2b	21	∞	0.125	15	0	∞
2023	31	2b	21	∞	0.125	45	0	∞
2051	28	2b	22	∞	0.4	0	0	∞
2052	28	2b	22	∞	0.25	0	0	∞
2053	28	2b	22	∞	0.167	0	0	∞
2054	28	2b	22	∞	0.125	0	0	∞
2055	28	2b	22	∞	0.076	0	0	∞
2056	28	2b	22	∞	0.065	0	0	∞
4001	20	2c	23,24	170	0.25	90	90	∞
4002	20	2c	23,24	170	0.125	90	90	∞
4003	20	2c	25,26,29	800	0.25	90	90	∞
4004	20	2c	25,26	800	0.125	90	90	∞
4005	20	2c	25,26	683	0.083	90	90	∞
4007	20	2c	27,28,29	3200	0.25	90	90	∞
4008	20	2c	27,28	3200	0.125	90	90	∞
4009	20	2c	27,28	3200	0.083	90	90	∞
4010	20	2c	27,28,29	3200	0.063	90	90	∞
4021	41	2c	30	24.6	0.535	90	90	35500
4023	41	2c	30	22.7	0.496	90	90	2469
4025	41	2c	31	20.1	0.50	90	90	∞
4027	41	2c	31	17.2	0.54	90	90	∞
4028	41	2c	32	22.9	0.493	90	90	1127
4034	41	2c	32	22.6	0.486	90	90	3559

Figure 6 presents the center line temperature and velocity decay for a simple momentum jet. The experimental data are obtained from the works of Albertson et al.,[3] Abramovich,[10] Becker et al.,[5] and Wygnanski and Fiedler.[6] The predictions are excellent, which is not surprising since the value for a_1 used here is obtained from these experiments.

Measurements show that for this flow the jet half-width grows linearly with x, that is, $r_{0.5} = K \cdot x$, with K ranging from 0.085 to 0.097. The predictions give K = 0.095, which is within the range of experimental values.

Figures 7 and 8 show the center line velocity and temperature decay and the jet half-width for three nonbuoyant jets discharged to a coflowing stream studied by Landis and Shapiro.[8] The predicted and experimental velocity and temperature decay rates are in good agreement. However, the predictions are shifted to the right relative to the data, which suggests that the starting length correlation proposed by Abramovich[10] (see Appendix D) may overestimate the starting length. Also, the predicted half-width values are somewhat less than the experimental values for $r_{0.5}$.

Figure 9 shows the maximum height of rise data and theoretical predictions for 40 buoyant jets discharged vertically upward into stably stratified ambients. The experimental data are due to Crawford and Leonard,[17] Abraham and Eysink,[18] Fox,[19] and Fan.[20] The theory is quite good, although it tends to slightly underpredict the experimental data. To demonstrate the importance of the a_2/Fr_L term in the entrainment function, predictions with a_2 = 0.0 are shown for some flows. Clearly, incorporation of this buoyancy-dependent term improves the accuracy of the predictions.

Figures 10–18 show predictions for buoyant jets discharged at various angles into uniform, quiescent ambients. Comparisons between Fan's[20] center line trajectory data and our predictions are shown in Figs.

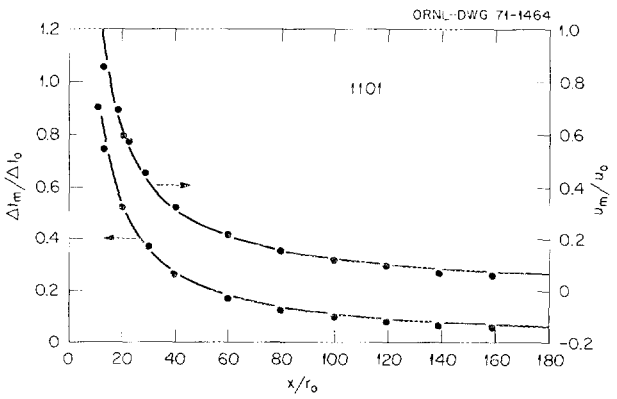

Fig. 6. Center line temperature and velocity decay for the simple momentum jet.

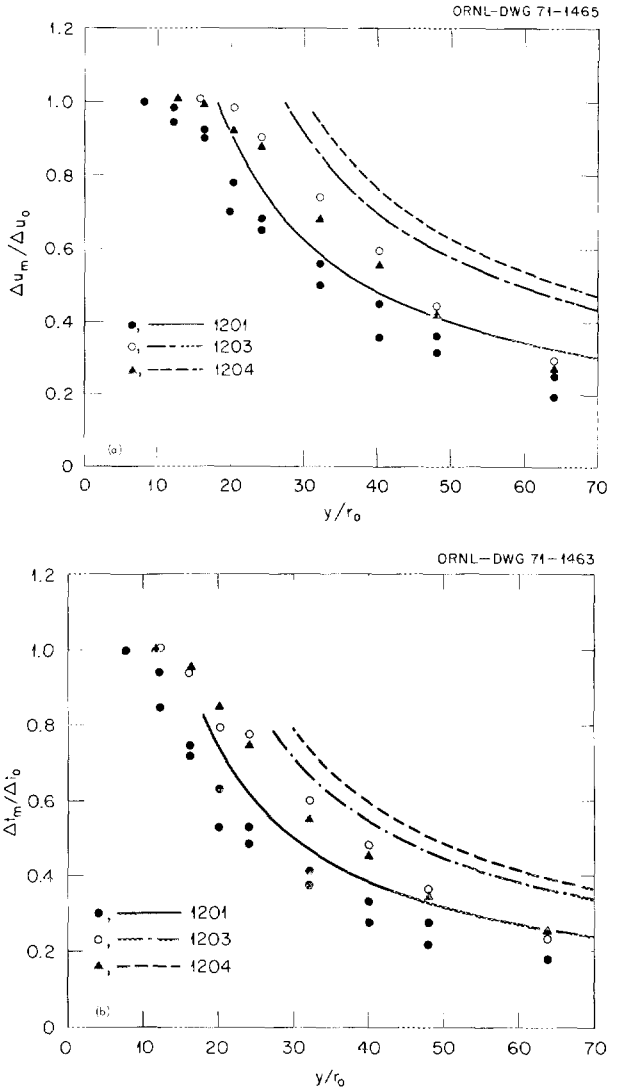

Fig. 7. (*a*) Center line velocity decay for nonbuoyant jets discharged to a coflowing stream; (*b*) center line temperature decay for nonbuoyant jets discharged to a coflowing stream.

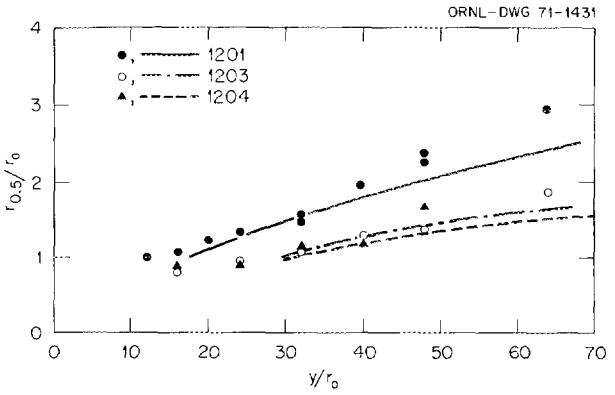

Fig. 8. Momentum half-width for nonbuoyant jets discharged to a coflowing stream.

10 and 11. The predictions lag behind the data, suggesting that a higher entrainment coefficient is needed. Predictions obtained with $a_1 = 0.082$ (the value Fan suggested) provide excellent agreement with the experimental trajectories for these flows; see Fig. 11. Unfortunately, using $a_1 = 0.82$ worsens the predictions for many other flows. So, for all other computations presented here, $a_1 = 0.057$, as indicated earlier.

Figures 12 and 13 illustrate the predictions for four buoyant jets discharged horizontally to a quiescent medium studied by Anwar.[26] The center line trajectory predictions are quite good. The center line concentration predictions are also good, but they tend to decay faster than the actual concentration.

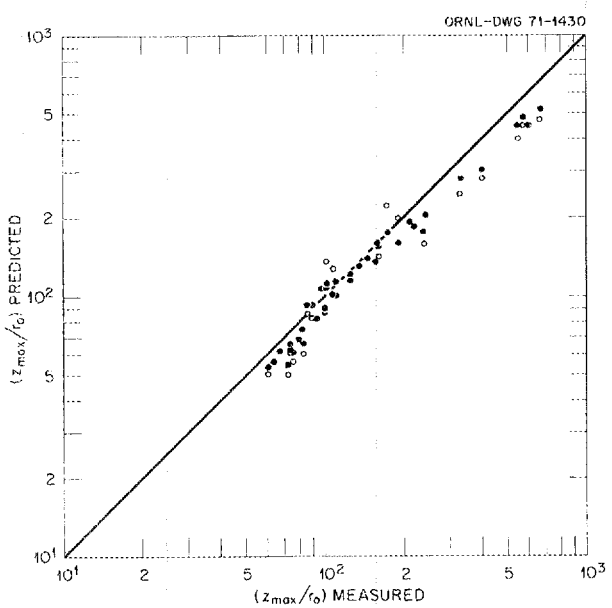

Fig. 9. Maximum height of rise for vertical plumes discharged to stratified ambients. (•) $a_2 = 0.97$; (○) $a_2 = 0.0$.

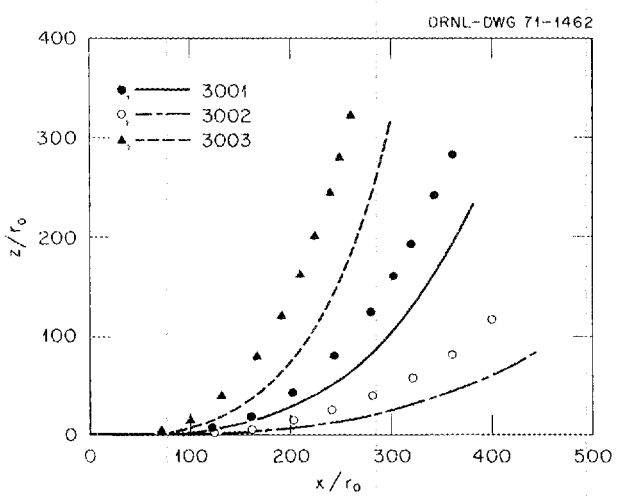

Fig. 10. Trajectories for horizontally discharged buoyant jets (data from ref. 20).

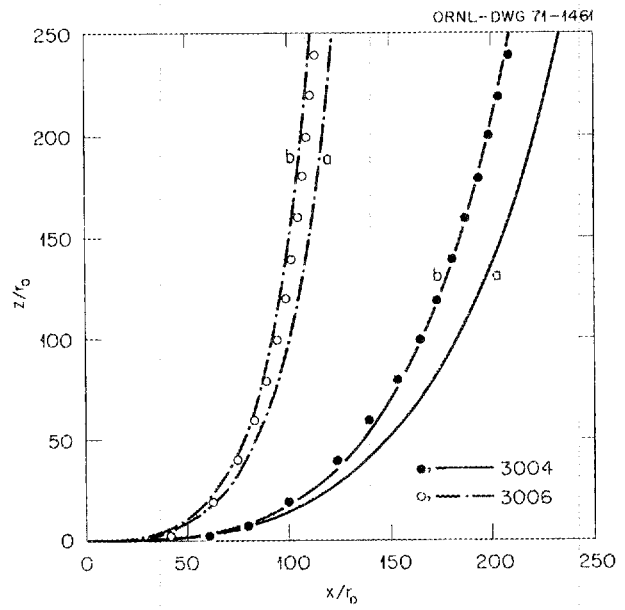

Fig. 11. Trajectories for horizontally discharged buoyant jets (data from ref. 20). (a) $a_1 = 0.057$; (b) $a_1 = 0.082$.

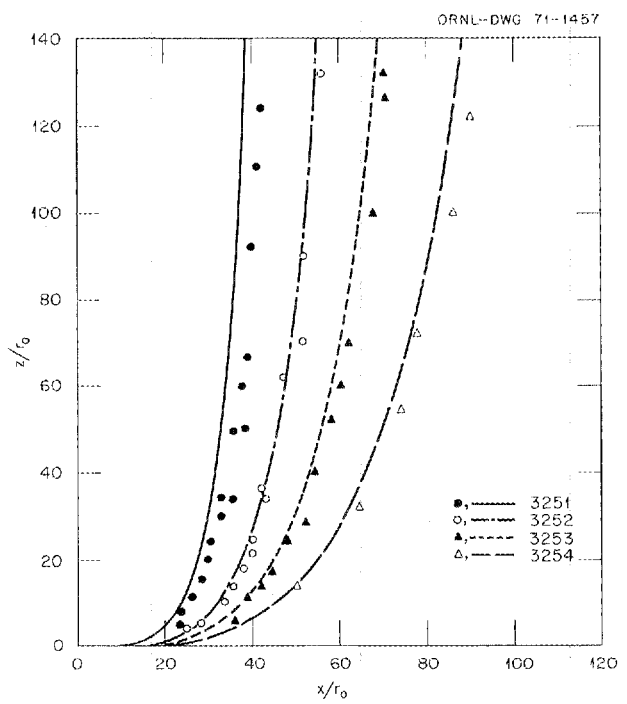

Fig. 12. Trajectories for horizontally discharged buoyant jets (data from ref. 26).

Figures 14–16 show comparisons between the center line concentration measurements of Frankel and Cumming[15] and the predictions for jets discharged at three different angles to the horizontal. In general, the predictions are quite accurate.

Figures 17 and 18 show center line trajectories for several buoyant jets discharged at various angles to stably stratified ambients studied by Fan.[20] As with Fan's data for jets discharged to a uniform ambient (Figs. 10 and 11), these predictions lag behind the data. Nevertheless, the predicted height-of-rise values are in close agreement with Fan's measurements.

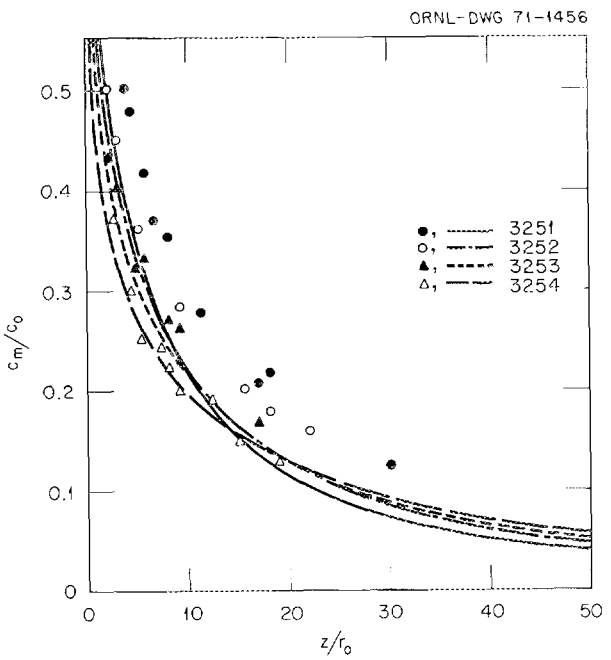

Fig. 13. Center line concentration decay for the horizontally discharged buoyant jets shown in Fig. 12.

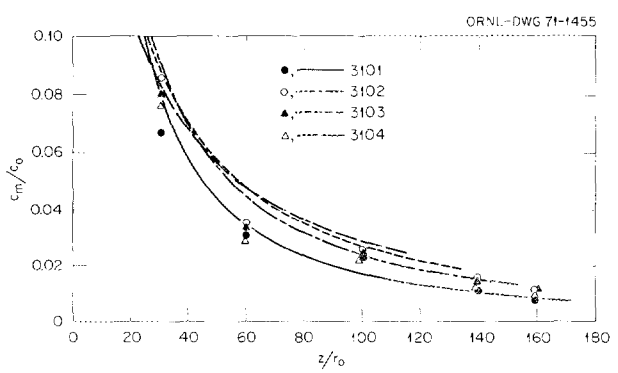

Fig. 14. Center line concentration decay for buoyant jets discharged with $\theta_2 = 0$ (data from ref. 15).

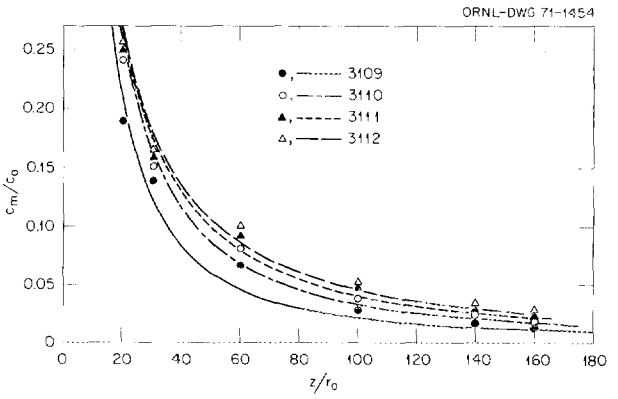

Fig. 15. Center line concentration decay for buoyant jets discharged with $\theta_2 = 30°$ (data from ref. 15).

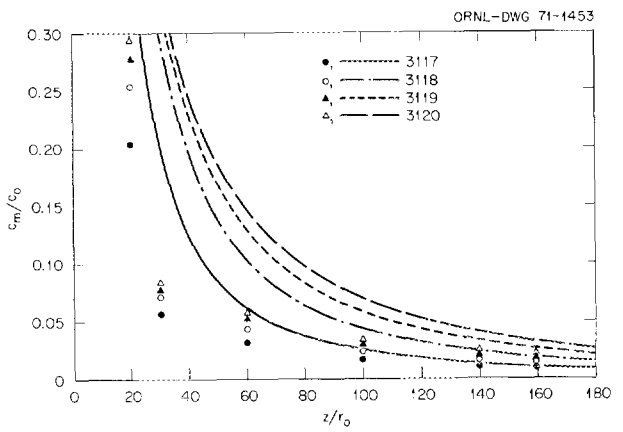

Fig. 16. Center line concentration decay for buoyant jets discharged with $\theta_2 = 90°$ (data from ref. 15).

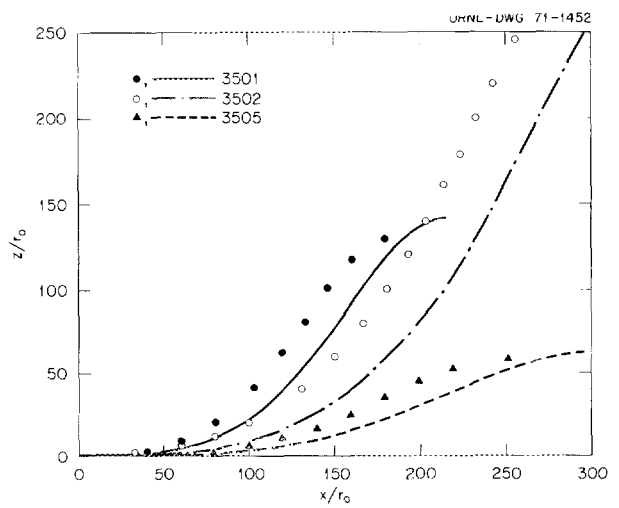

Fig. 17. Trajectories for buoyant jets discharged horizontally to stratified ambients (data from ref. 20).

The above results indicate that good agreement between theory and experiment can be obtained with the entrainment coefficients determined a priori and held constant.

Turning our attention now to flows for which $R \neq 0$ or $S_1 C_2 \neq 1$, we find that one constant, a_5, remains to be determined. This constant has been evaluated for both entrainment equations, (74) and (75), by calculating jet trajectories for several flows and adjusting the value of a_5 to provide a good fit. This method is somewhat subjective, in that the user's eye is used to decide when the best value has been reached.

Two important conclusions emerge from this "optimization" procedure. First, Eq. (74) provides much better predictions than does Eq. (75). Second, changing a_5 from its optimum value improves the predictions for some flows but worsens the predictions for others. The value finally selected for the entrainment equation (74) is

$$a_5 = 9.0 \,. \tag{77}$$

This gives, for the entrainment function used in all further predictions,

$$E = \left(0.057 + \frac{0.97}{\mathrm{Fr}_L} S_2\right) \left[b|u_m - u_{12}| + 9.0\, u_\infty b \sqrt{1 - (S_1 C_2)^2} \right] . \tag{78}$$

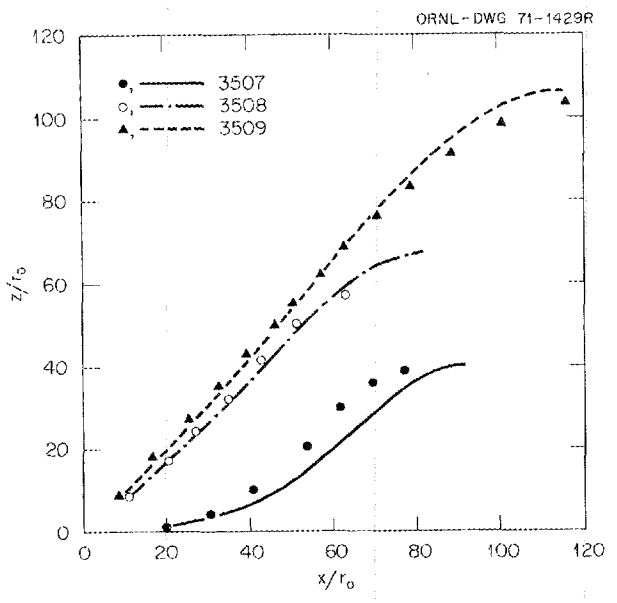

Fig. 18. Trajectories for buoyant jets discharged at various angles to stratified ambients (data from ref. 20).

Predictions have been made for 32 jets discharged to a cross flow. Comparisons between experimental data and theoretical predictions are shown in Figs. 19–32; see Table 1.

The measured and predicted trajectories for several nonbuoyant jets discharged to a cross flow are presented in Figs. 19–22. Figures 19–21 show a comparison between predictions and trajectories measured by Platten and Keffer[31] for jets discharged at various angles to a cross flow. The initial discharge angle varies from $\theta_1 = -45°$ to $+45°$. Except for the high cross-flow cases ($R = 0.25$), the predictions are reasonably good.

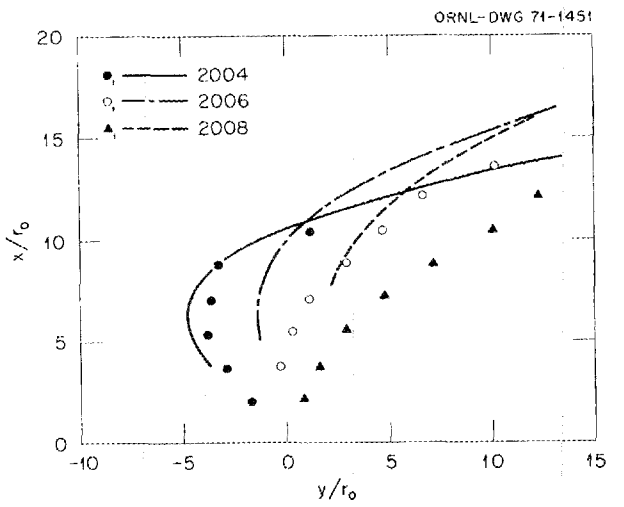

Fig. 19. Trajectories for nonbuoyant jets discharged at various angles to a free stream with $R = 0.25$ (data from ref. 31).

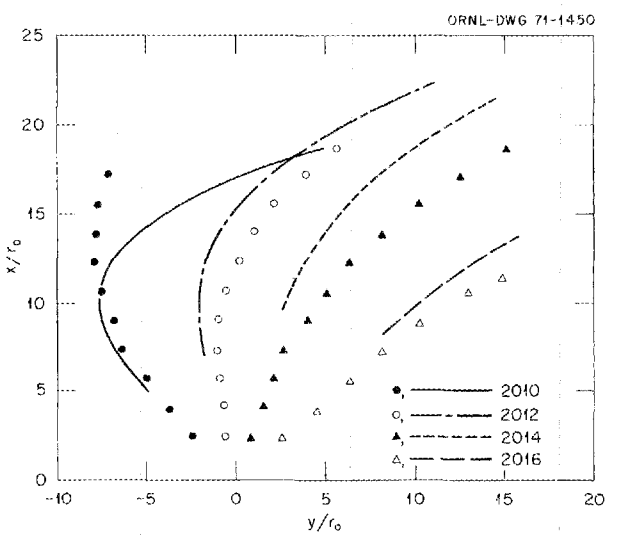

Fig. 20. Trajectories for nonbuoyant jets discharged at various angles to the free stream with $R = 0.167$ (data from ref. 31).

However, they tend to lag behind the actual trajectories, which suggests that either a_5 should be increased or that the jet orientation at s_e is not the same as at $s = 0$, as assumed in Appendix D.

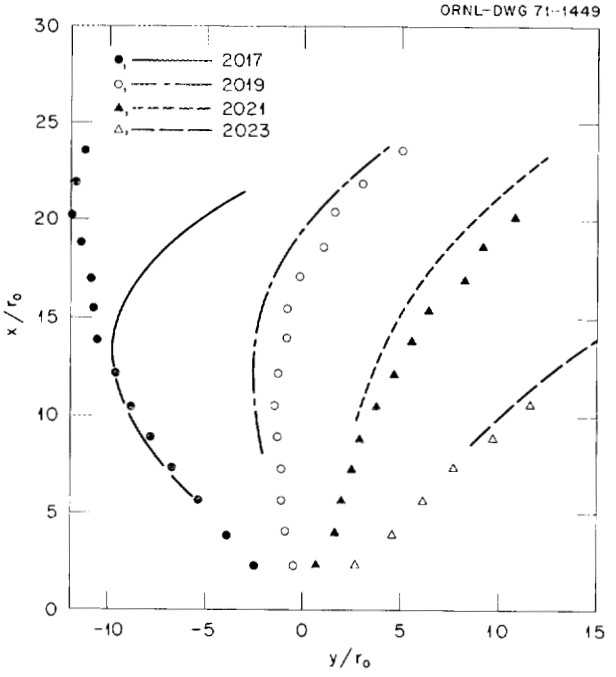

Fig. 21. Trajectories for nonbuoyant jets discharged at various angles to the free stream with $R = 0.125$ (data from ref. 31).

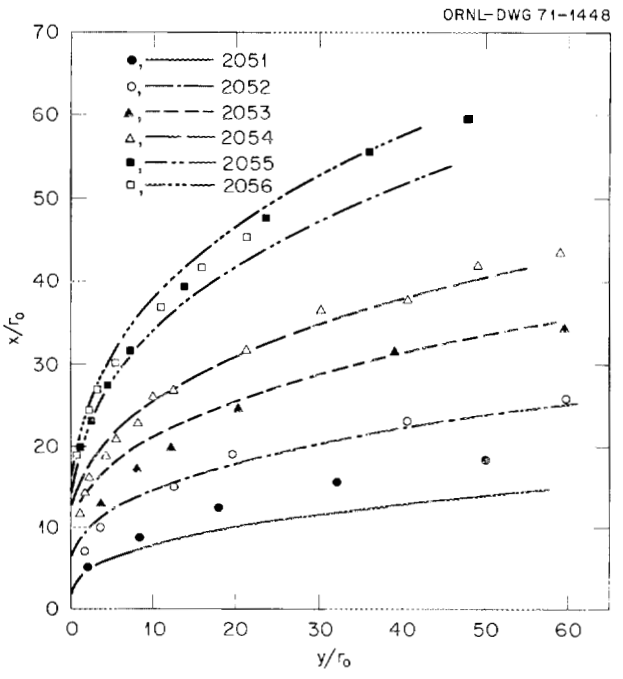

Fig. 22. Trajectories for nonbuoyant jets discharged normal to a cross flow (data from ref. 28).

Predictions and experimental data are compared in Fig. 22 for several jets discharged normal to a cross flow, with R ranging from 0.065 to 0.40. The predictions for these flows, measured by Gordier,[28] are quite good.

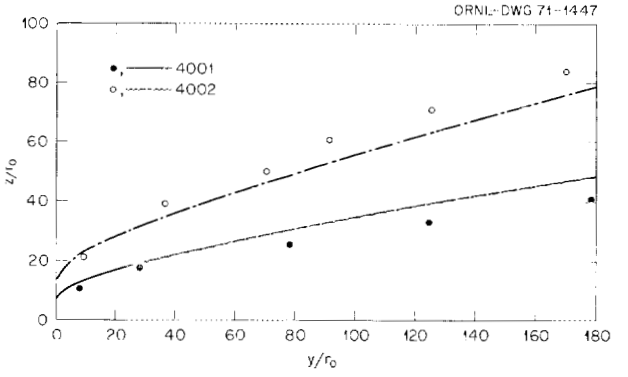

Fig. 23. Trajectories for buoyant jets discharged normal to a cross flow with Fr = 170 (data from ref. 20).

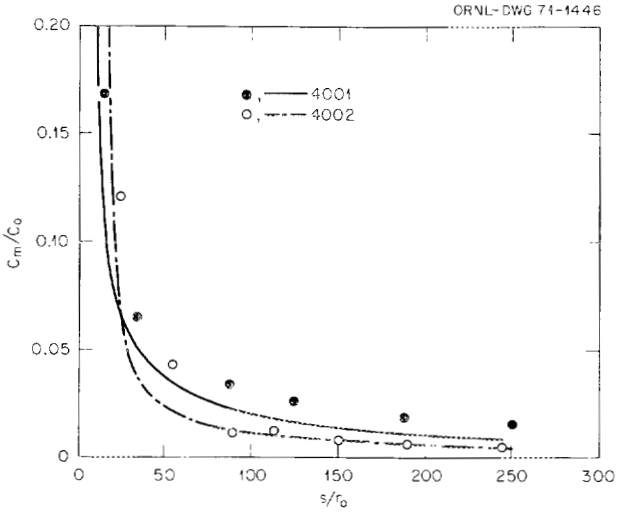

Fig. 24. Center line concentration decay for the buoyant jets discharged to a cross flow shown in Fig. 23.

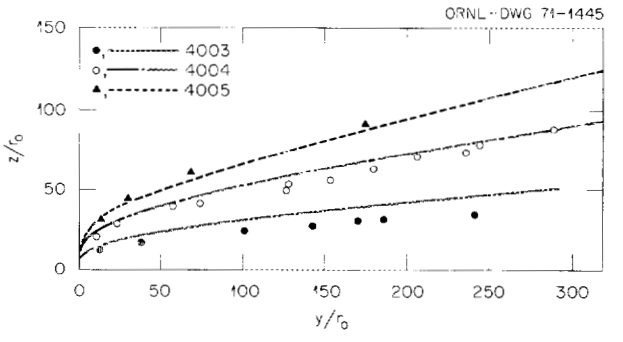

Fig. 25. Trajectories for buoyant jets discharged normal to a cross flow (data from ref. 20).

Results for buoyant jets discharged to a cross flow are presented in Figs. 23–32. Figures 23, 25, and 27 present comparisons between Fan's[20] trajectory measurements and the integral method predictions. The predictions are quite good. However, the theory tends to lag behind the data for large velocity ratios and lead slightly for smaller R.

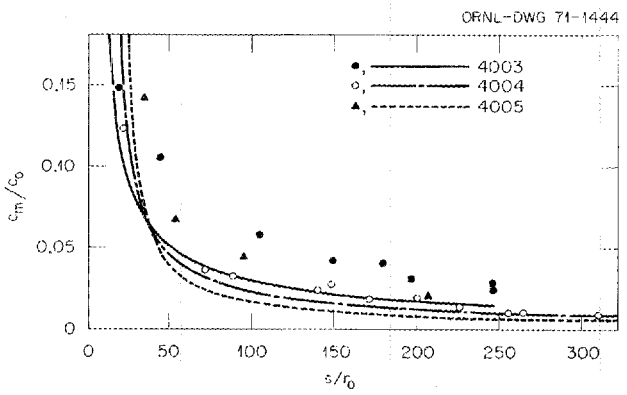

Fig. 26. Center line concentration decay for the buoyant jets discharged to a cross flow shown in Fig. 25.

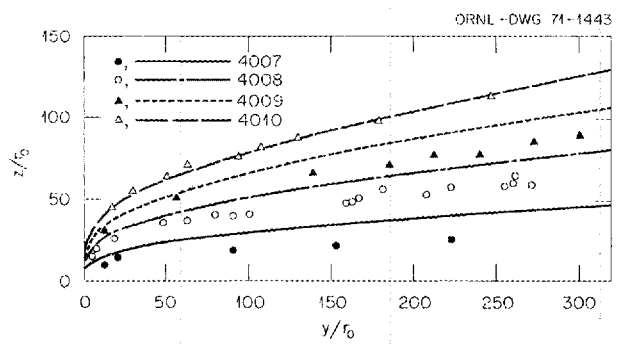

Fig. 27. Trajectories for buoyant jets discharged normal to a cross flow with Fr = 3200 (data from ref. 20).

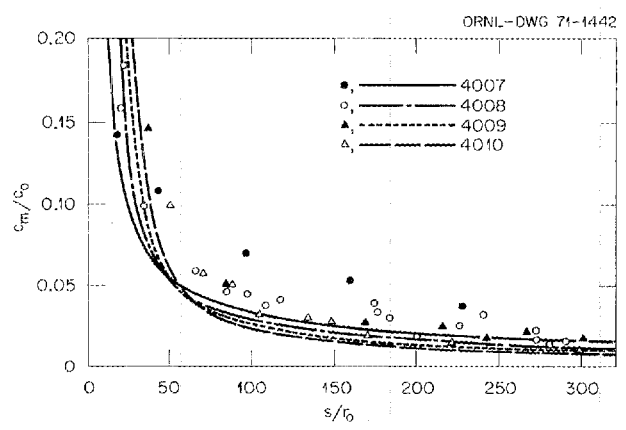

Fig. 28. Center line concentration decay for the buoyant jets discharged to a cross flow shown in Fig. 27.

Figures 24, 26, and 28 present comparisons between the center line concentration measurements and predictions for the same flows. Again, the predictions are good, although they tend to predict lower concentrations than those observed.

Figure 29 shows the predicted and measured half-widths for three of these flows. The agreement is adequate, but the predicted values of $r_{0.5}$ are consistently higher than are the experimental values. This is to be expected because of the discrepancy between the axisymmetric Gaussian profiles used in the predictions and the asymmetric vortex pairs observed.

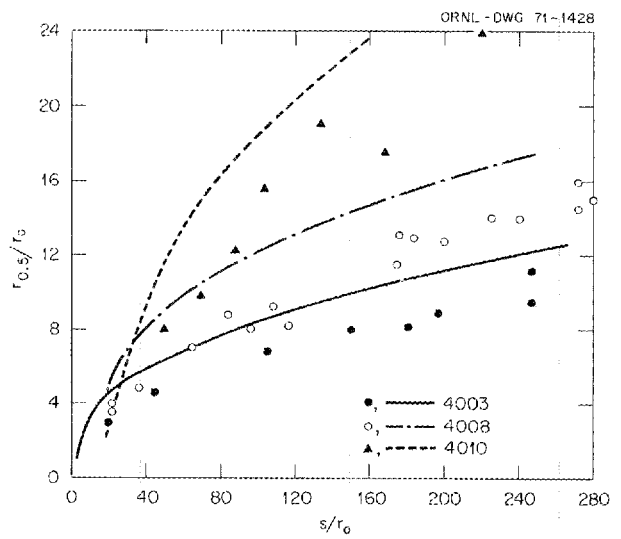

Fig. 29. Momentum half-width for some of the buoyant jets discharged to a cross flow shown in Figs. 23–28.

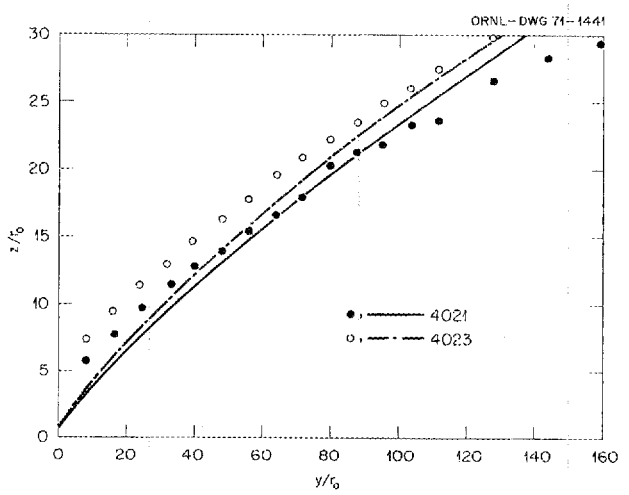

Fig. 30. Trajectories for buoyant jets discharged normal to a cross flow with stratified ambients (data from ref. 41).

Figures 30–32 present comparisons between the trajectories observed by Hewett and those predicted with the integral method. Except for the flows shown in Fig. 31 these jets were discharged to stably stratified ambients. The trajectory predictions are quite good.

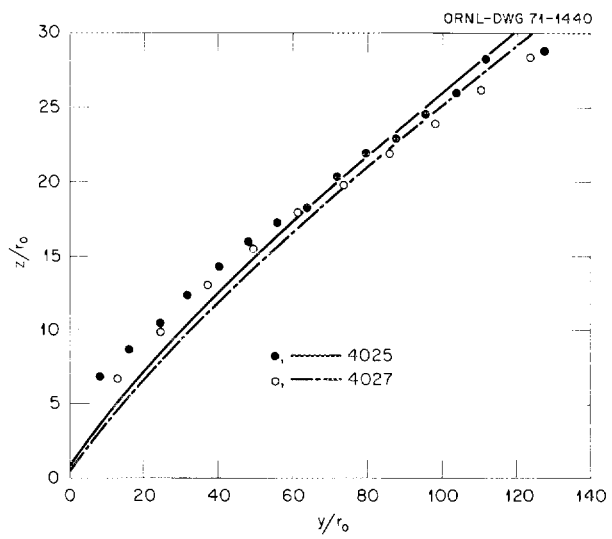

Fig. 31. Trajectories for buoyant jets discharged normal to a cross flow (data from ref. 41).

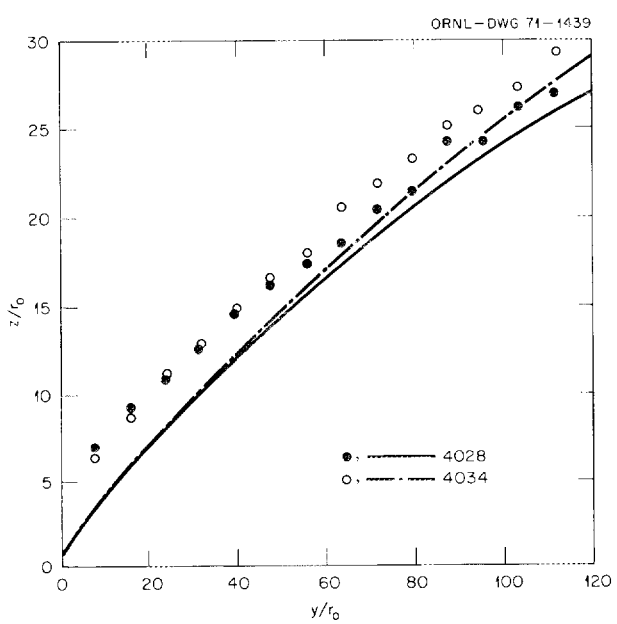

Fig. 32. Trajectories for buoyant jets discharged normal to a cross flow with stratified ambients (data from ref. 41).

4.4 Summary

A generalized integral method has been developed, based on the equations derived in Chap. 3. This new method is capable of predicting class 3 flows (as well as the simpler class 1 and 2 flows).

In order to achieve closure with this method the integrals have been evaluated using Gaussian profiles, and a new entrainment function has been postulated. This new entrainment equation, an extension of work by Fox[19] and Hoult et al.,[35] includes the effects of local conditions within the jet, free-stream velocity, and jet buoyancy. Three of the four entrainment coefficients are determined prior to comparison between theory and experiment. One is set intuitively and two are determined from experimental end points — the simple momentum jet and the simple plume. Only the fourth constant is determined by fitting the predictions to the data.

Theoretical results have been compared with experimental data for 103 class 1 and class 2 flows. As Table 1 shows, the range in experimental conditions is quite large. The Froude number ranges from 10 to ∞, the velocity ratio varies from 0 to 0.54, θ_1 varies from −45 to +45°, θ_2 varies from 0 to 90°, and the stratification parameter T ranges from 57 to ∞.

In general, the quality of predictions is "good" but not "excellent." The quality for certain flows can be improved by adjusting one or more of the entrainment coefficients, but this has not been done here. The predictions made with this new method are often no better than those made with existing methods. However, one must remember that the entrainment coefficients have been kept constant for *all* the flows studied and that this method should be capable of predicting class 3 flows, something which previous methods cannot do.

5. APPLICATIONS OF THE NEW METHOD

The method developed in Chaps. 3 and 4 is capable of predicting the growth and development of buoyant jets discharged at arbitrary angles to a flowing stratified ambient. In this chapter we shall see how the method can be used to predict the physical properties associated with thermal discharges from power plants. To illustrate the full generality of the method we shall assume that our hypothetical power plant is sited offshore on the continental shelf.* The effects of a cross flow and both thermal and salinity gradients will be considered.

*See the recent article by Anderson[51] for a discussion of the potential advantages of siting nuclear power plants in the ocean.

The physical properties of the ocean have been measured by numerous investigators; see reports by Sastry and Okubo,[47] Thomson et al.,[48] Cayot and North,[49] and Wiegel.[50] The reported measurements show the extreme variability of these properties with both time and space. For the purposes of illustration we shall site our power plant in the northern Gulf of California and use the temperature and salinity gradients presented in Figs. 10 and 16 of ref. 48. Averages of the April 1956, 1957, and 1959 data give, for the temperature and salinity gradients,

$$dt_\infty/dz = 0.030°\text{F/ft} ,$$

$$dc_\infty/dz = 0.00085 \text{ ppt/ft} ,*$$

with the surface temperature and salinity:

$$t_{\infty_o} = 65.8°\text{F} ,$$

$$c_{\infty_o} = 35.48 \text{ ppt} .$$

We shall assume that the power plant condenser inlet is located 100 m (328 ft) beneath the surface of the ocean and that the cooling water is discharged 50 m (164 ft) beneath the surface through a single 16-ft-diam round pipe.

With these assumptions the properties of the cooling water as it enters the condenser are:

$$t_{in} = 56.1°\text{F} ,$$

$$c_{in} = 35.20 \text{ ppt} .$$

Similarly, the free-stream properties at the outfall are:

$$t_{\infty_o} = 61.1°\text{F} ,$$

$$c_{\infty_o} = 35.34 \text{ ppt} ,$$

$$\rho_{\infty_o} = 64.0523 \text{ lb/ft}^3 , .$$

where the density is determined from Eq. (42) with

$$\beta = 0.00012 \, (°\text{F})^{-1} ,$$

$$\gamma = -0.00077 \, (\text{ppt})^{-1} .$$

*ppt = parts per thousand.

The reference density is taken as 64.0530 lb/ft^3 at 59.0°F and 35.00 ppt. These values of β and γ agree quite well with the experimental density measurements of salt water reported by Cox et al.[52] and Zerbe and Taylor.[53]

For a 1000-MW power plant operating at 33% efficiency, 2000 MW are discharged to the ocean as heated condenser cooling water. Thus

$$Q = 2000 \text{ MW} = 6.8 \times 10^9 \text{ Btu/hr} .$$

Since $Q = \rho c_p \, \Delta t \, \dot{V}$ and $\rho = 64.05$ lb/ft^3, $c_p = 0.96$ Btu lbm^{-1} (°F)$^{-1}$, then

$$\Delta t \, \dot{V} \cong 3.0 \times 10^4 \text{ ft}^3 \text{ °F sec}^{-1} ,$$

which shows that either the flow rate, $\dot{V}$, or the temperature difference, Δt, can be arbitrarily adjusted. For this example we shall consider two different combinations of flow rate and temperature difference:

1. $\Delta t = 10°$F. Then $\dot{V} = 3.0 \times 10^3$ ft^3/sec. Since $\dot{V} = \pi r_o^2 u_o$ and $r_o = 8$ ft, then $u_o = 14.9$ ft/sec.

The temperature, salinity, and density of the heated effluent as it leaves the outfall pipe are:

$$t_o = 56.1 + 10.0 = 66.1°\text{F} ,$$

$$c_o = c_{in} = 35.20 \text{ ppt} ,$$

$$\rho_o = 64.0037 \text{ lb/ft}^3 \text{ from Eq. (42)} .$$

Thus, the Froude number is:

$$\text{Fr} = \frac{(14.9)^2}{(8)\,(32.2)\,(64.0523 - 64.0037)/64.0037} = 1135.$$

Assuming the current to be 2.0 ft/sec gives, for the velocity ratio,

$$R = 2.0/14.9 = 0.134 .$$

2. $\Delta t = 20°$F. Now $\dot{V} = 1.5 \times 10^3$ ft^3/sec and $u_o = 7.5$ ft/sec.

The temperature, salinity, and density of the heated effluent as it leaves the outfall pipe are:

$$t_o = 76.1°\text{F} ,$$

$$c_o = 35.20 \text{ ppt} ,$$

$\rho_o = 63.9205$ lb/ft^3 .

The Froude number and velocity ratio are:

Fr = 106 ,

$R = 0.267$.

For both flow-rate–temperature-difference combinations, predictions have been computed for 12 different outfall conditions including discharge to a quiescent and flowing ocean at various initial angles. The 24 different cases considered are listed in Table 2. Flows are computed for jets discharging at 0, 45, and 90° to the horizontal with and without cross flows. In addition, when $R \neq 0$, flows are computed for jets which are discharged with $\theta_1 = -30$, 0, and +30°. These cases include a wide range of operating conditons.

Table 2 and Figs. 33–36 can be used to help develop an optimum discharge configuration for this situation. The fifth and sixth columns in Table 2 give the volumes of water within the jet for which the temperature difference (above local ambient) is greater than the value indicated. The last column in this table lists the temperature difference between the jet and ambient at the water surface.

Figures 33–36 show the trajectories for 8 of the 24 configurations considered here. Figure 33 shows trajectories for three jets discharged to a quiescent ocean, with Δt = 10°F, at angles of 0, 45, and 90° to the

Table 2. Thermal discharge configurations from a hypothetical power plant

Δt_o = 10°F, u_o = 14.9 ft/sec, Fr = 1135, T = 29.3

ID No.	R	θ_1 (deg)	θ_2 (deg)	$V_{\Delta t=3°}$ (10^4 ft^3)	$V_{\Delta t=2°}$ (10^4 ft^3)	$\Delta t_{m,\text{surf.}}$[a] (°F)
9001	0	0	0	2.49	6.83	*b*
9002	0	0	45	2.15	3.94	−1.5
9003	0	0	90	2.07	3.69	0
9004	0.134	0	0	1.66	3.49	*b*
9005	0.134	0	45	1.57	2.79	−2.0
9006	0.134	90	90	1.56	2.74	−1.4
9007	0.134	−30	0	1.66	3.70	*b*
9008	0.134	−30	45	1.49	2.71	−3.5
9009	0.134	90	120	1.52	2.74	−2.5
9010	0.134	30	0	1.72	3.64	*b*
9011	0.134	30	45	1.65	2.90	−1.9
9012	0.134	90	60	1.62	2.83	−1.5

Δt_o = 20°F, u_o = 7.5 ft/sec, Fr = 106, T = 79.3

ID No.	R	θ_1 (deg)	θ_2 (deg)	$V_{\Delta t=10°}$ (10^4 ft^3)	$V_{\Delta t=6°}$ (10^4 ft^3)	$\Delta t_{m,\text{surf.}}$[a] (°F)
9013	0	0	0	1.90	6.20	−3.7
9014	0	0	45	1.81	4.59	+2.0
9015	0	0	90	1.79	4.36	+4.5
9016	0.267	0	0	*c*	1.87	*b*
9017	0.267	0	45	*c*	1.55	*b*
9018	0.267	90	90	*c*	1.54	−1.8
9019	0.267	−30	0	0.739	2.04	*b*
9020	0.267	−30	45	*c*	1.48	*b*
9021	0.267	90	120	0.727	1.77	−2.1
9022	0.267	30	0	*c*	2.68	*b*
9023	0.267	30	45	*c*	2.06	*b*
9024	0.267	90	60	*c*	2.44	−1.0

[a] $\Delta t_{m,\text{surf.}} = t_{m,\text{surface}} - t_{\infty,\text{surface}}$.

[b] The jet does not reach the water surface for these cases.

[c] The volume within which $\Delta t > 10°$ is completely inside the potential core.

horizontal. The dashed lines on Fig. 33 indicate the regions within which the jet center line temperature is greater (or less) than the local ambient temperature. Because the ocean is stably stratified there is a region in which the jet is actually cooler than the surrounding ocean. This figure shows that jet location and extent are strongly dependent on the initial angle of discharge.

Figure 34 shows trajectories for three jets discharged to a quiescent ocean with $\Delta t = 20°F$. The initial Froude number is much smaller for these flows than for the jets shown in Fig. 33. Consequently, these jets rise more rapidly and the temperature excess is greater than for the high Fr jets.

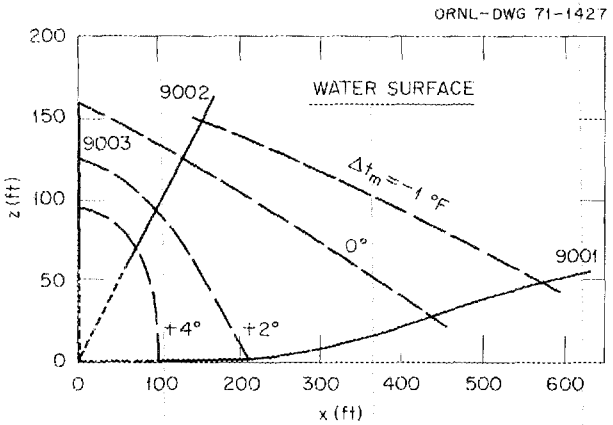

Fig. 33. Trajectories for thermal jets discharged from a hypothetical power plant to a quiescent ocean; Δt_o = 10°F, Fr = 1135, T = 29.3.

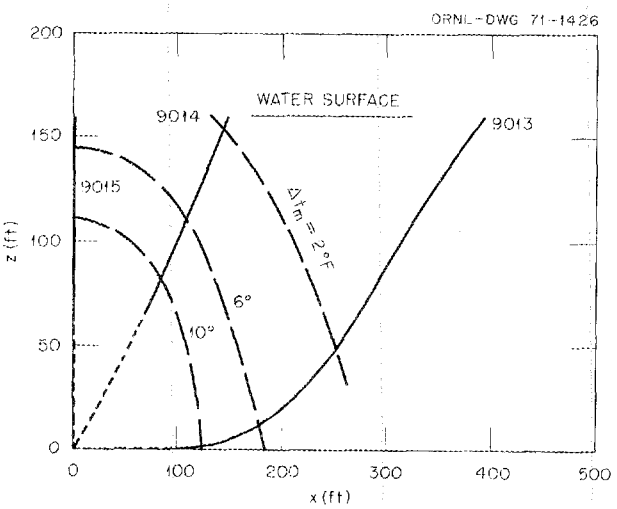

Fig. 34. Trajectories for thermal jets discharged from a hypothetical power plant to a quiescent ocean; Δt_o = 20°F, Fr = 106, T = 79.3.

Figures 35 and 36 show trajectories for jets discharged in a vertical plane at various angles to the free stream (θ_2 = 60, 90, and 120°). These figures show that the lower Fr flows (Fig. 36) are deflected more rapidly than are the higher Fr flows (Fig. 35).

Several observations and conclusions can be drawn from these predictions:

1. Discharge with Δt = 10°F and u_o = 14.9 ft/sec gives much smaller mixing zones (regions in which the jet temperature is significantly higher than the ambient temperature) than does discharge with Δt = 20°F and u_o = 7.5 ft/sec. However, the larger flow rate associated with the smaller Δt implies a higher pumping cost. In addition, the higher velocities may adversely affect the fish near the diffuser outfall and increase the entrainment of organisms.

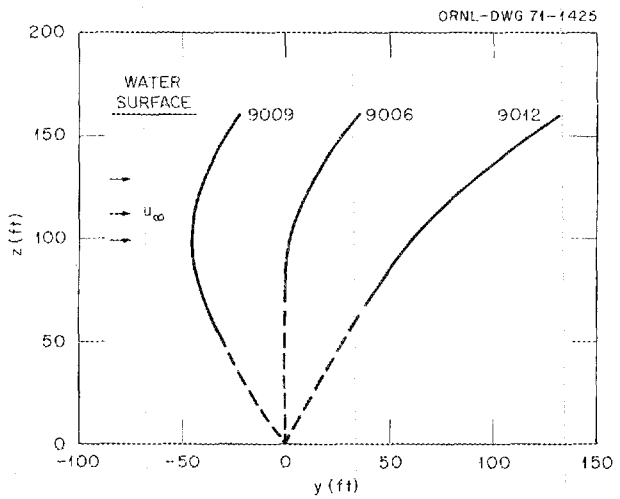

Fig. 35. Trajectories for thermal jets discharged from a hypothetical power plant to an ocean current; Δt_o = 10°F, Fr = 1135, T = 29.3, R = 0.134.

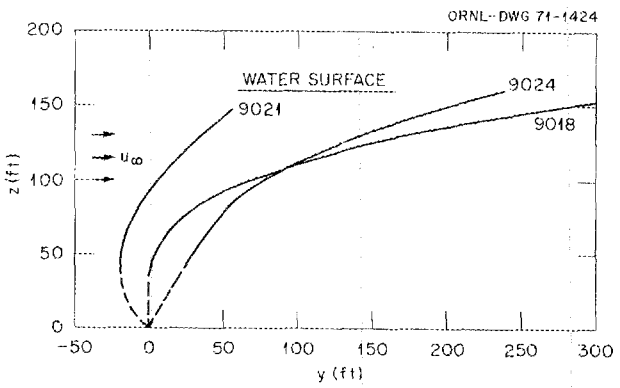

Fig. 36. Trajectories for thermal jets discharged from a hypothetical power plant to an ocean current; Δt_o = 20°F, Fr = 106, T = 79.3, R = 0.267.

2. For jets discharged to the quiescent ($R = 0$) stratified ambient the mixing zone is smallest for vertical discharge and largest for horizontal discharge. This is because of the higher entrainment coefficient associated with larger values of θ_2. However, at a fixed height the temperature increase is greatest due to the vertically discharged jet; see Figs. 33 and 34. The importance of this depends on the levels at which various aquatic organisms live.

3. The effect of a cross flow ($R \neq 0$) is to substantially reduce the size of the mixing zone; see Table 2. Thus, discharge to a quiescent ambient is the worst possible case.

4. For both temperature differences the smallest mixing zones are obtained with jets discharged at $\theta_1 = -30°$ and $\theta_2 = 45°$. This suggests that jets discharged at an oblique angle to the free stream yield the smallest mixing zones. On the other hand, the largest mixing zones are obtained with horizontally discharged jets. Thus, for rapid heat dissipation the jets should be discharged at an angle of $\theta_2 \cong 45°$.

5. Those jets discharged upstream at an oblique angle to the free stream affect the smallest total region in the ocean. For example, Figs. 35 and 36 show that jets 9008 and 9020 have shorter trajectories than do the other jets shown.

6. For discharge with $\Delta t = 10°F$ most of the jets reach the water surface, while for discharge with $\Delta t = 20°F$ only half the jets reach the surface. Since the atmosphere is the ultimate sink of this thermal energy it is important to be able to predict the heat transfer rates for the jet after it has reached the surface. The theory discussed here cannot do this. One complicating factor is that the jet center line temperature at the surface is usually less than the ambient surface temperature because of the stratification.

These results show that, if rapid mixing and dispersion of the heated effluent are desired, discharge should be at $\theta_1 = -30°$ and $\theta_2 = 45°$ with $\Delta t = 10°F$. If, on the other hand, rapid heat exchange with the atmosphere is desired then the jet should be discharged vertically up with $\Delta t = 20°F$. The relative desirability of these two extremes depends, to a large extent, on the ecological consequences of these discharge configurations.

In an actual power plant design one would calculate the mixing zones and trajectories for many more configurations than we have done here. In addition one would have to consider several different sets of ambient conditions to find those which give the worst ecological effects. However, the example presented here gives a "feel" for the utility of this new integral method.

6. SUMMARY AND RECOMMENDATIONS

The new method developed in Chaps. 3 and 4 is unique in several ways. The basic integral equations (45) to (50), derived in Chap. 3 and the Appendices, are written in a general form which allows the method to predict flows with three-dimensional trajectories (class 3 flows), as well as the flows with single plane trajectories (class 1 and 2 flows) which other methods can predict. Derivation of these integral equations from the basic partial differential equations reveals new terms involving the ambient turbulence and the radius of curvature which do not appear in other integral methods. These additional terms are important for jets discharged to a turbulent ambient and for jets discharged to a cross flow in the region where the curvature is large.

In Chap. 4, a new generalized entrainment function is developed, based on the works of Fox[19] and Hoult et al.[35] This new formulation includes the effects of internal turbulence, cross flow, and buoyancy on the entrainment rate and contains four coefficients, only one of which is determined empirically by fitting the predictions to the data.

The theoretical predictions are compared with data for about 100 different flows. The agreement between theory and experiment is quite good, which is especially significant since the method has been used to predict a very wide range of flows with all four entrainment coefficients kept constant.

Additional experimental and theoretical work is needed to improve predictions of temperature profiles in heated discharges and to increase the generality of this method. Some specific recommendations follow.

6.1 Future Experimental Study

As indicated in Chaps. 2 and 4, experimental data exist only for class 1 and 2 flows. Experimental data for class 3 flows are needed in order to test the general validity of the new integral method. The most immediate need is for data concerning jet trajectories, center line temperature and velocity decay, and temperature and velocity profiles normal to the jet axis for several class 3 flows. These data can then be used to assess the accuracy of the new method. If the method is found wanting then the data can be used to help develop an improved entrainment function.

Detailed turbulence measurements have been made only for the simple momentum jet. Because the buoyant jet flows studied here are inherently turbulent, there is a real need for experimental data concerning the turbulent structure of flows other than the simple momentum jet.

In order to assess the ability of this new method to predict jet development in a turbulent ambient some experiments performed with jets discharged to a turbulent ambient should be performed.

6.2 Future Theoretical Analyses

The entrainment function (78) used in this method appears to work reasonably well. However, more accurate entrainment formulations can probably be developed. One could relate the entrainment to an integral measure of the turbulence intensity. Then, a model of the turbulent kinetic energy equation could be used to predict the development of this turbulence parameter. This approach, which involves the use of a differential equation rather than an algebraic equation for the entrainment, has been explored to some extent by Telford.[42]

Another possibility is to integrate the partial differential equations (C-17) to (C-22) rather than the integral equations. With the partial differential equations no assumptions concerning the velocity and temperature profiles must be made. On the other hand, the various turbulence terms appearing in these equations must be specified in terms of the mean-flow variables. Work of this nature is being carried out at a few institutions on similar problems. A search of the literature, however, failed to reveal any attempts to solve buoyant jet problems using the partial differential equations.

There are several ways in which the new method should be extended. The method is capable of predicting jet growth and development only in the zone of established flow. The method can be extended to the zone of flow establishment using the profiles suggested by Albertson et al.[3] More important, the method should be extended to allow prediction of the jet's development after it has reached its ultimate height. These extensions should be general enough to allow predictions of the jet development before the momentum is depleted (surface jet) and when the fluid moves with the ambient (field zone).

In general, interest in thermal discharges is centered on the biological effects rather than the physical effects of the thermal discharge. Therefore, attempts should be made to couple the method developed here with "thermal-death" models. These biological models are capable of predicting fish mortality, loss of equilibrium, and susceptibility to predation given the time-temperature history of the fish. This time-temperature history can be obtained from the method developed here. Thus, the outputs from the integral method serve as inputs to the biological model. Such an integrated mathematical model can then be used to predict certain ecological consequences of thermal discharges through single submerged diffusers.

Appendix A

THE s, r, ϕ COORDINATE SYSTEM

Figure 5 shows the coordinate system used in this analysis. x, y, z are the usual Cartesian coordinates and $\mathbf{i}, \mathbf{j}, \mathbf{k}$ are the corresponding unit vectors. z is the vertical coordinate and y is set parallel to the ambient current.

s, r, ϕ are the coordinates in the natural system with $\mathbf{i}_s$, $\mathbf{i}_r$, $\mathbf{i}_\phi$ the corresponding unit vectors. s measures the distance along the jet axis from the origin (diffuser exit) and $\mathbf{i}_s$ is always tangent to the center line. r measures the distance from the jet axis in a plane perpendicular to $\mathbf{i}_s$; $r = 0$ along the axis. ϕ is the angle which determines the orientation of r. The convention adopted sets $\phi = 0$ when $\mathbf{i}_r$ is horizontal to the left with ϕ increasing in the clockwise direction, looking in the direction of increasing s.

With these definitions s, r, ϕ form a right-handed system of orthogonal curvilinear coordinates. At any fixed s, r and ϕ are the usual cylindrical polar coordinates.

The two coordinate systems are related to each other by θ_1 and θ_2. θ_1 measures the angle between the projection of $\mathbf{i}_s$ onto the x, y plane and the x axis. If there is no cross flow then θ_1 remains constant along the jet axis.

θ_2 measures the angle between $\mathbf{i}_s$ and the x, y plane and varies in response to both buoyancy forces and the cross flow.

The relationships among the unit vectors of the two coordinate systems are shown schematically in Table A-1. Two examples suffice to illustrate the use of this table.

$$\mathbf{i}_s = C_1 C_2 \mathbf{i} + S_1 C_2 \mathbf{j} + S_2 \mathbf{k} ,$$

$$\mathbf{j} = S_1 C_2 \mathbf{i}_s + (C\phi C_1 - S\phi S_1 S_2)\mathbf{i}_r - (S\phi C_1 + C\phi S_1 S_2)\mathbf{i}_\phi .$$

The basic differential equations, (37) to (39) and (44), are written in terms of the gradient, divergence, and curl. These vector differential operators can be defined for this coordinate system only after the scale factors have been derived.

The scale factors, h_s, h_r, and h_ϕ, are:

$$h_s = \frac{\partial \mathbf{R}}{\partial s} \cdot \mathbf{i}_s ,$$

$$h_r = \frac{\partial \mathbf{R}}{\partial r} \cdot \mathbf{i}_r ,$$

Table A-1. Relationships among the unit vectors in Cartesian and natural coordinate systems

	i	j	k
$\mathbf{i}_s$	C_1C_2	S_1C_2	S_2
$\mathbf{i}_r$	$-(C\phi S_1 + S\phi C_1 S_2)$	$C\phi C_1 - S\phi S_1 S_2$	$S\phi C_2$
$\mathbf{i}_\phi$	$S\phi S_1 - C\phi C_1 S_2$	$-(S\phi C_1 + C\phi S_1 S_2)$	$C\phi C_2$

$C_i = \cos\theta_i$ $\quad$ $S_i = \sin\theta_i$

$C\phi = \cos\phi$ $\quad$ $S\phi = \sin\phi$

$$h_\phi = \frac{\partial \mathbf{R}}{\partial \phi}\cdot \mathbf{i}_\phi ,$$

where $\mathbf{R} = s\mathbf{i}_s + r\mathbf{i}_r$ is the position vector of any point in the jet. The scale factors relate the differential distances to the differentials of the coordinates. In general, they vary from point to point. Only for the Cartesian coordinate system are the scale factors constant. To evaluate h_s we proceed as follows:

$$\frac{\partial \mathbf{R}}{\partial s} = \mathbf{i}_s + s\frac{\partial \mathbf{i}_s}{\partial s} + \frac{\partial r}{\partial s}\mathbf{i}_r + r\frac{\partial \mathbf{i}_r}{\partial s},$$

$$\frac{\partial \mathbf{R}}{\partial s}\cdot \mathbf{i}_s = 1 + 0 + 0 + r\frac{\partial \mathbf{i}_r}{\partial s}\cdot \mathbf{i}_s .$$

Using the relationships in Table A-1:

$$\frac{\partial \mathbf{i}_r}{\partial s} = \frac{\partial \mathbf{i}_r}{\partial \theta_1}\frac{1}{\rho_1} + \frac{\partial \mathbf{i}_r}{\partial \theta_2}\frac{1}{\rho_2} = \frac{1}{\rho_1}\left[-(C\phi C_1 - S\phi S_1 S_2)\mathbf{i} - (C\phi S_1 + S\phi C_1 S_2)\mathbf{j}\right] - \frac{1}{\rho_2}\left[S\phi C_1 C_2 \mathbf{i} + S\phi S_1 C_2 \mathbf{j} + S\phi S_2 \mathbf{k}\right] .$$

Finally,

$$h_s = 1 + r\frac{\partial \mathbf{i}_r}{\partial s}\cdot \mathbf{i}_s = 1 - r\left(\frac{C\phi C_2}{\rho_1} + \frac{S\phi}{\rho_2}\right) \triangleq 1 - e . \quad \text{(A-1)}$$

Similarly,

$$h_r = 1 , \quad \text{(A-2)}$$

$$h_\phi = r . \quad \text{(A-3)}$$

From page 137 of ref. 54, the gradient is:

$$\nabla a = \frac{1}{h_s}\frac{\partial a}{\partial s}\mathbf{i}_s + \frac{1}{h_r}\frac{\partial a}{\partial r}\mathbf{i}_r + \frac{1}{h_\phi}\frac{\partial a}{\partial \phi}\mathbf{i}_\phi , \quad \text{(A-4)}$$

where a is any scalar. Substituting the scale factor expressions into (A-4) yields:

$$\nabla a = \frac{1}{1-e}\frac{\partial a}{\partial s}\mathbf{i}_s + \frac{\partial a}{\partial r}\mathbf{i}_r + \frac{1}{r}\frac{\partial a}{\partial \phi}\mathbf{i}_\phi . \quad \text{(A-5)}$$

The divergence[54] of a vector $\mathbf{a}$ is:

$$\nabla\cdot\mathbf{a} = \frac{1}{h_s h_r h_\phi}\left[\frac{\partial(h_r h_\phi a_s)}{\partial s} + \frac{\partial(h_\phi h_s a_r)}{\partial r} + \frac{\partial(h_s h_r a_\phi)}{\partial \phi}\right], \quad \text{(A-6)}$$

where $\mathbf{a} = a_s\mathbf{i}_s + a_r\mathbf{i}_r + a_\phi\mathbf{i}_\phi$. Substituting the scale factor expressions into (A-6) yields:

$$\nabla\cdot\mathbf{a} = \frac{1}{1-e}\frac{\partial a_s}{\partial s} + \frac{1}{r}\frac{\partial(ra_r)}{\partial r} + \frac{1}{r}\frac{\partial a_\phi}{\partial \phi} - \frac{a_r}{1-e}\left[\frac{e}{r}\right] - \frac{a_\phi}{1-e}\left[\frac{1}{r}\frac{\partial e}{\partial \phi}\right] . \quad \text{(A-7)}$$

The curl[54] of a vector $\mathbf{a}$ is

$$\nabla\times\mathbf{a} = \frac{1}{h_s h_r h_\phi}\begin{vmatrix} h_s\mathbf{i}_s & h_r\mathbf{i}_r & h_\phi\mathbf{i}_\phi \\ \frac{\partial}{\partial s} & \frac{\partial}{\partial r} & \frac{\partial}{\partial \phi} \\ h_s a_s & h_r a_r & h_\phi a_\phi \end{vmatrix} . \quad \text{(A-8)}$$

Substituting the scale factor expressions into (A-8) yields:

$$\nabla\times\mathbf{a} = \frac{1}{r}\left[\frac{\partial(ra_\phi)}{\partial r} - \frac{\partial a_r}{\partial \phi}\right]\mathbf{i}_s + \left[\frac{1}{r}\frac{\partial a_s}{\partial \phi} - \frac{a_s}{1-e}\left(\frac{1}{r}\frac{\partial e}{\partial \phi}\right) - \frac{1}{1-e}\frac{\partial a_\phi}{\partial s}\right]\mathbf{i}_r + \left[\frac{1}{1-e}\frac{\partial a_r}{\partial s} - \frac{\partial a_s}{\partial r} + \frac{a_s}{1-e}\left(\frac{e}{r}\right)\right]\mathbf{i}_\phi . \quad \text{(A-9)}$$

These expressions for the gradient (A-5), divergence (A-7), and curl (A-9) are used in Appendix B to derive the governing equations for the jet from the original vector equations, (37) to (39) and (44).

Appendix B

THE BASIC EQUATIONS IN TERMS OF s, r, ϕ

Using the expressions for the gradient, divergence, and curl derived in Appendix A, Eqs. (37) to (39) and (44) become, when written in scalar form:

continuity equation, (37):

$$\frac{1}{1-e}\frac{\partial u}{\partial s}+\frac{1}{r}\frac{\partial(r\mathrm{v})}{\partial r}+\frac{1}{r}\frac{\partial w}{\partial\phi}-\frac{\mathrm{v}}{1-e}\frac{e}{r}-\frac{w}{1-e}\frac{1}{r}\frac{\partial e}{\partial\phi}=0\ ; \quad \text{(B-1)}$$

energy equation, (38):

$$\frac{u}{1-e}\frac{\partial t}{\partial s}+\mathrm{v}\frac{\partial t}{\partial r}+\frac{w}{r}\frac{\partial t}{\partial\phi}=0\ ; \quad \text{(B-2)}$$

concentration equation, (39):

$$\frac{u}{1-e}\frac{\partial c}{\partial s}+\mathrm{v}\frac{\partial c}{\partial r}+\frac{w}{r}\frac{\partial c}{\partial\phi}=0\ ; \quad \text{(B-3)}$$

s momentum equation [Eq. (44)$\cdot\mathbf{i}_s$]:

$$\frac{u}{1-e}\frac{\partial u}{\partial s}+\mathrm{v}\frac{\partial u}{\partial r}+\frac{w}{r}\frac{\partial u}{\partial\phi}-\frac{uw}{1-e}\frac{1}{r}\frac{\partial e}{\partial\phi}-\frac{u\mathrm{v}}{1-e}\frac{e}{r}=\frac{\rho_\infty-\rho}{\rho_0}gS_2-\frac{\nabla p^*\cdot\mathbf{i}_s}{\rho_0}\ ; \quad \text{(B-4)}$$

r momentum equation [Eq. (44)$\cdot\mathbf{i}_r$]:

$$\frac{u}{1-e}\frac{\partial\mathrm{v}}{\partial s}+\mathrm{v}\frac{\partial\mathrm{v}}{\partial r}+\frac{w}{r}\frac{\partial\mathrm{v}}{\partial\phi}-\frac{w^2}{r}+\frac{u^2}{1-e}\frac{e}{r}=\frac{\rho_\infty-\rho}{\rho_0}gS\phi C_2-\frac{\nabla p^*\cdot\mathbf{i}_r}{\rho_0}\ ; \quad \text{(B-5)}$$

ϕ momentum equation [Eq. (44)$\cdot\mathbf{i}_\phi$]:

$$\frac{u}{1-e}\frac{\partial w}{\partial s}+\mathrm{v}\frac{\partial w}{\partial r}+\frac{w}{r}\frac{\partial w}{\partial\phi}+\frac{\mathrm{v}w}{r}+\frac{u^2}{1-e}\frac{1}{r}\frac{\partial e}{\partial\phi}=\frac{\rho_\infty-\rho}{\rho_0}gC\phi C_2-\frac{\nabla p^*\cdot\mathbf{i}_\phi}{\rho_0}\ . \quad \text{(B-6)}$$

Equations (B-1) to (B-6) are a set of six nonlinear coupled partial differential equations with three independent variables — s, r, ϕ. The eight unknowns are u, v, w, p^*, t, c, θ_1, and θ_2. The density, $\rho(t, c)$, is found from the algebraic equation of state, (43).

Two additional kinematical conditions are required to close the system. These conditions arise from our definition of the jet center line. Requiring the velocity at $r = 0$ to be parallel to the center line (i.e., the center line is a streamline) yields:

$$\mathrm{v}(s, 0, 0) = w(s, 0, 0) = 0\ . \quad \text{(B-7)}$$

In addition, we require the velocity at any s station to be a maximum or minimum at the center line:

$$\left.\frac{\partial\bar{\mathrm{v}}}{\partial r}\right)_{r=0}=0\ . \quad \text{(B-8)}$$

This yields a system of three linear homogeneous algebraic equations for $(\partial u/\partial r)_{r=0}$, $(\partial\mathrm{v}/\partial r)_{r=0}$, and $(\partial w/\partial r)_{r=0}$. Since the determinant of the coefficient matrix is not, in general, zero, then the three partial derivatives must be zero:

$$\left.\frac{\partial u}{\partial r}\right)_{r=0}=\left.\frac{\partial\mathrm{v}}{\partial r}\right)_{r=0}=\left.\frac{\partial w}{\partial r}\right)_{r=0}=0\ . \quad \text{(B-9)}$$

Thus, the definition of the center line as a streamline along which the velocity is locally a maximum gives five additional conditions, three of which can be used as boundary conditions.*

Additional boundary conditions are:

1. At $s = 0$,

$$u,\ \mathrm{v},\ w,\ p^*,\ t,\ c \text{ specified as } f_i(r, \phi)\ ,$$
$$\theta_1, \theta_2 \text{ specified}\ . \quad \text{(B-10)}$$

2. In the circumferential direction,

$$u,\ \mathrm{v},\ w,\ p^*,\ t,\ c(\phi) = u,\ \mathrm{v},\ w,\ p^*,\ t,\ c(\phi + 2\pi)\ . \quad \text{(B-11)}$$

3. In the radial direction:

a) As $r \to$ infinity,†

$$\nabla p^* \to 0,\quad t \to t_\infty,\quad c \to c_\infty,$$
$$u \to u_\infty S_1 C_2\ ,$$
$$\mathrm{v} \to u_\infty(C\phi C_1 - S\phi S_1 S_2)\ ,$$
$$w \to -u_\infty(S\phi C_1 + C\phi S_1 S_2)\ . \quad \text{(B-12)}$$

*These conditions, Eqs. (B-7) and (B-9), are somewhat arbitrary. For jets in a cross flow the actual flow pattern is similar to a vortex pair, in which case the appropriate kinematic conditions are different. Since these conditions are not required for the solution developed here, this point is not discussed further.

†Conditions (B-12) neglect possible variations of u_∞, t_∞, and c_∞ around the jet perimeter.

b) At $r = 0$,

See Eqs. (B-7) and (B-9).

Appendix C

DERIVATION OF THE AXISYMMETRIC EQUATIONS

In order to simplify the equations developed in Appendix B, we shall assume the flow to be axisymmetric, that is, $w = 0$, $\partial/\partial\phi = 0$. Also the nonhydrostatic pressure gradient, ∇p^*, is neglected.

The ϕ momentum equation, (B-6), is meaningless for axisymmetric flow. Therefore, rather than write momentum equations in the s, r, and ϕ directions, we shall write them in the s, z, and y directions. This will give us momentum equations parallel to the jet axis, parallel to the buoyancy force, and parallel to the free stream.

The k momentum equation is:

$$k \text{ equation} = (\text{B-4})\cdot S_2 + (\text{B-5})\cdot S\phi C_2 + (\text{B-6})\cdot C\phi C_2 ,$$

or:

$$\begin{aligned}
&\frac{u}{1-e}\left(\frac{\partial u}{\partial s}S_2 + \frac{\partial v}{\partial s}S\phi C_2 + \frac{\partial w}{\partial s}C\phi C_2\right) \\
&\quad + v\left(\frac{\partial u}{\partial r}S_2 + \frac{\partial v}{\partial r}S\phi C_2 + \frac{\partial w}{\partial r}C\phi C_2\right) \\
&\quad + \frac{w}{r}\left(\frac{\partial u}{\partial \phi}S_2 + \frac{\partial v}{\partial \phi}S\phi C_2 + \frac{\partial w}{\partial \phi}C\phi C_2\right) \\
&\quad - \frac{w}{r}\left(u\frac{\partial e}{\partial \phi}\frac{S_2}{1-e} + wS\phi C_2 - vC\phi C_2\right) \\
&\quad + \frac{u}{(1-e)r}\left(-veS_2 + ueS\phi C_2 \right. \\
&\qquad \left. + u\frac{\partial e}{\partial \phi}C\phi C_2\right) = \frac{\rho_\infty - \rho}{\rho_0}g . \qquad \text{(C-1)}
\end{aligned}$$

Similarly, the j momentum equation is:

$$j \text{ equation} = (\text{B-4})\cdot S_1 C_2 + (\text{B-5})\cdot(C\phi C_1 - S\phi S_1 S_2) - (\text{B-6})\cdot(S\phi C_1 + C\phi S_1 S_2) ,$$

or:

$$\begin{aligned}
&\frac{u}{1-e}\left[\frac{\partial u}{\partial s}S_1 C_2 + \frac{\partial v}{\partial s}\left(C\phi C_1 - S\phi S_1 S_2\right)\right. \\
&\quad \left. - \frac{\partial w}{\partial s}\left(S\phi C_1 + C\phi S_1 S_2\right)\right] + v\left[\frac{\partial u}{\partial r}S_1 C_2\right. \\
&\quad \left. + \frac{\partial v}{\partial r}\left(C\phi C_1 - S\phi S_1 S_2\right) - \frac{\partial w}{\partial r}\left(S\phi C_1 + C\phi S_1 S_2\right)\right] \\
&\quad + \frac{w}{r}\left[\frac{\partial u}{\partial \phi}S_1 C_2 + \frac{\partial v}{\partial \phi}\left(C\phi C_1 - S\phi S_1 S_2\right)\right. \\
&\quad \left. - \frac{\partial w}{\partial \phi}\left(S\phi C_1 + C\phi S_1 S_2\right)\right] - \frac{w}{r}\left[\frac{u}{1-e}\frac{\partial e}{\partial \phi}S_1 C_2\right. \\
&\quad \left. + w\left(C\phi C_1 - S\phi S_1 S_2\right) + v\left(S\phi C_1 + C\phi S_1 S_2\right)\right] \\
&\quad + \frac{u}{(1-e)r}\left[-veS_1 C_2 + ue\left(C\phi C_1 - S\phi S_1 S_2\right)\right. \\
&\qquad \left. - u\frac{\partial e}{\partial \phi}\left(S\phi C_1 + C\phi S_1 S_2\right)\right] = 0 . \qquad \text{(C-2)}
\end{aligned}$$

Multiplying Eqs. (B-1) to (B-4), (C-1), and (C-2) by $(1 - e)$, setting $w = 0$ and $\partial/\partial\phi = 0$, and integrating with respect to ϕ from 0 to 2π yields (assuming that all the dependent variables are independent of ϕ):

$$\frac{\partial u}{\partial s} + \frac{1}{r}\frac{\partial}{\partial r}(rv) = 0 , \qquad \text{(C-3)}$$

$$u\frac{\partial t}{\partial s} + v\frac{\partial t}{\partial r} = 0 , \qquad \text{(C-4)}$$

$$u\frac{\partial c}{\partial s} + v\frac{\partial c}{\partial r} = 0 , \qquad \text{(C-5)}$$

$$u\frac{\partial u}{\partial s} + v\frac{\partial u}{\partial r} = \frac{\rho_\infty - \rho}{\rho_0}gS_2 , \qquad \text{(C-6)}$$

$$\left(u\frac{\partial u}{\partial s} + v\frac{\partial u}{\partial r}\right)S_2 + \left(u^2 - \frac{rv}{2}\frac{\partial v}{\partial r}\right)\frac{C_2}{\rho_2} = \frac{\rho_\infty - \rho}{\rho_0}g , \qquad \text{(C-7)}$$

$$\left(u\frac{\partial u}{\partial s} + v\frac{\partial u}{\partial r}\right)S_1 C_2 + \left(u^2 - \frac{rv}{2}\frac{\partial v}{\partial r}\right) \times \left(\frac{C_1 C_2}{\rho_1} - \frac{S_1 S_2}{\rho_2}\right) = 0 . \qquad \text{(C-8)}$$

For the sake of completeness the i momentum equation is also given:*

*Only three of the four momentum equations, (C-6) to (C-9), are independent. Any one can be derived from the other three.

$$\left(u\frac{\partial u}{\partial s}+\mathrm{v}\frac{\partial u}{\partial r}\right)C_1C_2-\left(u^2-\frac{r\mathrm{v}}{2}\frac{\partial \mathrm{v}}{\partial r}\right)\times\left(\frac{S_1C_2}{\rho_1}+\frac{C_1S_2}{\rho_2}\right)=0\,. \qquad \text{(C-9)}$$

The above equations do not explicitly include the effects of turbulence. It is usual, for turbulent flows, to write the equations in terms of average and fluctuating quantities, that is,

$$f=\bar{f}+f'\,,$$

where $\bar{f}$ is the average value of f, defined as

$$\bar{f}=\lim_{\tau\to\infty}\left(\frac{1}{2\tau}\int_{-\tau}^{+\tau}f\,d\tau\right)\,,$$

and f' is the fluctuating component of f. By definition, $\overline{f'}=0$. Writing the dependent variables u, v, t, and c in terms of average and fluctuating components and plugging these expressions into Eqs. (C-3) to (C-9) yields:

$$\frac{\partial\bar{u}}{\partial s}+\frac{1}{r}\frac{\partial(r\bar{\mathrm{v}})}{\partial r}=0\,, \qquad \text{(C-10)}$$

$$\bar{u}\frac{\partial\bar{t}}{\partial s}+\bar{\mathrm{v}}\frac{\partial\bar{t}}{\partial r}=-\left[\frac{\partial(\overline{u't'})}{\partial s}+\frac{1}{r}\frac{\partial(r\overline{\mathrm{v}'t'})}{\partial r}\right], \qquad \text{(C-11)}$$

$$\bar{u}\frac{\partial\bar{c}}{\partial s}+\bar{\mathrm{v}}\frac{\partial\bar{c}}{\partial r}=-\left[\frac{\partial(\overline{u'c'})}{\partial s}+\frac{1}{r}\frac{\partial(r\overline{\mathrm{v}'c'})}{\partial r}\right]\,, \qquad \text{(C-12)}$$

$$\bar{u}\frac{\partial\bar{u}}{\partial s}+\bar{\mathrm{v}}\frac{\partial\bar{u}}{\partial r}=\frac{\rho_\infty-\bar{\rho}}{\rho_0}gS_2-\left[\frac{\partial(\overline{u'^2})}{\partial s}+\frac{1}{r}\frac{\partial(r\overline{u'\mathrm{v}'})}{\partial r}\right], \qquad \text{(C-13)}$$

$$\left(\bar{u}\frac{\partial\bar{u}}{\partial s}+\bar{\mathrm{v}}\frac{\partial\bar{u}}{\partial r}\right)S_2+\left(\bar{u}^2-\frac{r\bar{\mathrm{v}}}{2}\frac{\partial\bar{\mathrm{v}}}{\partial r}\right)\frac{C_2}{\rho_2}=\frac{\rho_\infty-\bar{\rho}}{\rho_0}g-\left[\frac{\partial\overline{u'^2}}{\partial s}+\frac{1}{r}\frac{\partial(r\overline{u'\mathrm{v}'})}{\partial r}\right]S_2-\left[\overline{u'^2}-\frac{r}{4}\frac{\partial\overline{\mathrm{v}'^2}}{\partial r}\right]\frac{C_2}{\rho_2}\,, \qquad \text{(C-14)}$$

$$\left(\bar{u}\frac{\partial\bar{u}}{\partial s}+\bar{\mathrm{v}}\frac{\partial\bar{u}}{\partial r}\right)S_1C_2+\left(\bar{u}^2-\frac{r\bar{\mathrm{v}}}{2}\frac{\partial\bar{\mathrm{v}}}{\partial r}\right)\times\left(\frac{C_1C_2}{\rho_1}-\frac{S_1S_2}{\rho_2}\right)=-\left[\frac{\partial\overline{u'^2}}{\partial s}+\frac{1}{r}\frac{\partial(r\overline{u'\mathrm{v}'})}{\partial r}\right]S_1C_2-\left(\overline{u'^2}-\frac{r}{4}\frac{\partial\overline{\mathrm{v}'^2}}{\partial r}\right)\left(\frac{C_1C_2}{\rho_1}-\frac{S_1S_2}{\rho_2}\right)\,, \qquad \text{(C-15)}$$

$$\left(\bar{u}\frac{\partial\bar{u}}{\partial s}+\bar{\mathrm{v}}\frac{\partial\bar{u}}{\partial r}\right)C_1C_2-\left(\bar{u}^2-\frac{r\bar{\mathrm{v}}}{2}\frac{\partial\bar{\mathrm{v}}}{\partial r}\right)\times\left(\frac{S_1C_2}{\rho_1}+\frac{C_1S_2}{\rho_2}\right)=-\left[\frac{\partial\overline{u'^2}}{\partial s}+\frac{1}{r}\frac{\partial(r\overline{u'\mathrm{v}'})}{\partial r}\right]C_1C_2+\left(\overline{u'^2}-\frac{r}{4}\frac{\partial\overline{\mathrm{v}'^2}}{\partial r}\right)\left(\frac{S_1C_2}{\rho_1}+\frac{C_1S_2}{\rho_2}\right)\,. \qquad \text{(C-16)}$$

The flow in a buoyant turbulent jet is of the boundary layer type; that is, gradients in the streamwise direction (s) are much smaller than in the normal direction (r), and $\bar{u}\gg\bar{\mathrm{v}}$. Using the boundary layer approximations due to Prandtl[4,5] the above equations reduce to:

$$\frac{\partial\bar{u}}{\partial s}+\frac{1}{r}\frac{\partial(r\bar{\mathrm{v}})}{\partial r}=0\,, \qquad \text{(C-17)}$$

$$\bar{u}\frac{\partial\bar{t}}{\partial s}+\bar{\mathrm{v}}\frac{\partial\bar{t}}{\partial r}=-\frac{1}{r}\frac{\partial(r\overline{\mathrm{v}'t'})}{\partial r}\,, \qquad \text{(C-18)}$$

$$\bar{u}\frac{\partial\bar{c}}{\partial s}+\bar{\mathrm{v}}\frac{\partial\bar{c}}{\partial r}=-\frac{1}{r}\frac{\partial(r\overline{\mathrm{v}'c'})}{\partial r}\,, \qquad \text{(C-19)}$$

$$\bar{u}\frac{\partial\bar{u}}{\partial s}+\bar{\mathrm{v}}\frac{\partial\bar{u}}{\partial r}=\frac{\rho_\infty-\bar{\rho}}{\rho_0}gS_2-\frac{1}{r}\frac{\partial(r\overline{u'\mathrm{v}'})}{\partial r}\,, \qquad \text{(C-20)}$$

$$\left(\bar{u}\frac{\partial\bar{u}}{\partial s}+\bar{\mathrm{v}}\frac{\partial\bar{u}}{\partial r}\right)S_2=\frac{\rho_\infty-\bar{\rho}}{\rho_0}g-q^*\frac{C_2}{\rho_2}-\frac{1}{r}\frac{\partial(r\overline{u'\mathrm{v}'})}{\partial r}S_2\,, \qquad \text{(C-21)}$$

$$\left(\bar{u}\frac{\partial\bar{u}}{\partial s}+\bar{\mathrm{v}}\frac{\partial\bar{u}}{\partial r}\right)S_1C_2=-q^*\left(\frac{C_1C_2}{\rho_1}-\frac{S_1S_2}{\rho_2}\right)-\frac{1}{r}\frac{\partial(r\overline{u'\mathrm{v}'})}{\partial r}S_1C_2\,, \qquad \text{(C-22)}$$

$$\left(\bar{u}\frac{\partial\bar{u}}{\partial s}+\bar{\mathrm{v}}\frac{\partial\bar{u}}{\partial r}\right)C_1C_2=+q^*\left(\frac{S_1C_2}{\rho_1}+\frac{C_1S_2}{\rho_2}\right)-\frac{1}{r}\frac{\partial(r\overline{u'\mathrm{v}'})}{\partial r}C_1C_2\,, \qquad \text{(C-23)}$$

where

$$q^*=\bar{u}^2-\frac{r}{4}\left(\frac{\partial\bar{\mathrm{v}}^2}{\partial r}+\frac{\partial\overline{\mathrm{v}'^2}}{\partial r}\right)\,.$$

Equations (C-17) to (C-22) are a set of six equations for $\bar{u}$, $\bar{\mathrm{v}}$, $\bar{t}$, $\bar{c}$, θ_1, θ_2, $\overline{u'\mathrm{v}'}$, $\overline{u'^2}$, $\overline{\mathrm{v}'^2}$, $\overline{\mathrm{v}'t'}$, and $\overline{\mathrm{v}'c'}$.

The turbulence quantities can be handled in different ways,[55] the most common of which is to assume that the "Reynolds stress" terms are simple functions of the mean quantities, for example,

$$\overline{u'v'} = \epsilon_m \frac{\partial \bar{u}}{\partial r},$$

$$\overline{v't'} = \epsilon_h \frac{\partial \bar{t}}{\partial r},$$

where ϵ_m and ϵ_h are the eddy viscosity for momentum and heat, respectively, and are prescribed functions. The boundary conditions for this problem are:

1. At $s = 0$,

   $\bar{u}, \bar{v}, \bar{t}, \bar{c}$ specified as $f_i(r)$,

   θ_1 and θ_2 specified.

2. As $r \to$ infinity,

   $\bar{u} \to u_\infty S_1 C_2$,

   $\bar{v} \to -E/r$,

   where

   $E = d/ds \int_0^\infty \bar{u} r\, dr$ is the entrainment rate,

   $\bar{t} \to t_\infty$,

   $\bar{c} \to c_\infty$.

3. At $r = 0$, certain boundary conditions may be required depending on the nature of the turbulence assumptions.

Appendix D

SPECIFICATION OF THE INITIAL CONDITIONS

Equations (58) to (63) can be used to develop theoretical solutions for class 3 jets once appropriate initial conditions are specified. These initial conditions are specified at the diffuser exit, the beginning of the zone of flow establishment ($s = 0$). However, the integral equations are valid only in the region of established flow. Therefore, we need to derive initial conditions at the end of the zone of flow establishment (at s_e) in terms of the diffuser outfall conditions (at $s = 0$).

In order to account for this initial region of flow development the length of the region, s_e, must be defined and the appropriate values for u_m, b, Δt_m, and Δc_m must be specified at s_e.

Abramovich[10] gives an expression for the length of this potential core for a nonbuoyant jet discharged to a *coflowing* stream. Adjusting his constant so that $s_e/r_o = 12.4$ when $R = 0$ (from Albertson[3]) gives:

$$s_e/r_o = 12.4 \left(\frac{1+R}{1-R}\right) \frac{1}{\sqrt{1+1.18R}}. \qquad \text{(D-1)}$$

Equation (D-1) shows that the starting length increases with increasing R, which is in accord with the observations of Shapiro and coworkers.[7,8]

Fan[20] graphically defines the starting length for jets discharged to a *cross* flow, based on Gordier's[28] data. Fan's correlation is closely approximated by:

$$s_e/r_o = 12.4 - 28.0R. \qquad \text{(D-2)}$$

Combining and generalizing Eqs. (D-1) and (D-2) yields an expression applicable to class 3 nonbuoyant jets:

$$s_e/r_o = 12.4 \left(\frac{1+R_{12}}{1-R_{12}}\right) \frac{1}{\sqrt{1+1.18R_{12}}} - 28.0R\sqrt{1-(S_1C_2)^2}. \qquad \text{(D-3)}$$

This equation is valid only for values of R less than about 0.5.

Abraham[13] gives a starting length expression for buoyant jets discharged vertically up into a quiescent medium. This equation, a cubic, shows that the starting length decreases from $12.4r_o$ as the Froude number decreases. Abraham's equation can be approximated by:

$$\begin{aligned} s_e/r_o &= 12.4, & \mathrm{Fr} &\geq 80, \\ &= 7.8 + 0.057\,\mathrm{Fr}, & 10 &\leq \mathrm{Fr} < 80, \\ &= 4.15 + 0.425\,\mathrm{Fr}, & 2 &\leq \mathrm{Fr} < 10, \\ &= 0, & 0 &\leq \mathrm{Fr} < 2. \end{aligned} \qquad \text{(D-4)}$$

Combining Eqs. (D-3) and (D-4) yields a general starting length equation valid for all class 3 flows:

$$s_e/r_o = \frac{(s_e/r_o)_{\text{D-3}}\,(s_e/r_o)_{\text{D-4}}}{12.4}. \qquad \text{(D-5)}$$

In order to define values of the dependent variables at s_e the following assumptions are made:

1. $u_m = u_o$ at $s = s_e$, by definition of s_e;
2. buoyancy forces are neglected in the zone of flow establishment;
3. the influence of free stream gradients (dt_∞/dz, dc_∞/dz) and free stream velocity are neglected in this region;
4. the jet orientation at s_e is assumed equal to that at $s = 0$, that is, $\theta_{1_e} = \theta_{1_o}$ and $\theta_{2_e} = \theta_{2_o}$.

Mass, momentum, energy, and salt balances between $s = 0$ and $s = s_e$ provide the following conditions:

$$u_m = u_o ,$$

$$b^2 = \frac{2u_o}{u_o + u_{12_o}} r_o^2 ,$$

$$\Delta t_m = \frac{\lambda^2 + 1}{2\lambda^2} \left(\frac{u_o + u_{12_o}}{u_o + \lambda^2 u_{12_o}} \right) \Delta t_o ,$$

$$\Delta c_m = \frac{\lambda^2 + 1}{2\lambda^2} \left(\frac{u_o + u_{12_o}}{u_o + \lambda^2 u_{12_o}} \right) \Delta c_o . \qquad \text{(D-6)}$$

These boundary conditions (D-6) are derived by assuming that the profiles are top-hat at $s = 0$ and Gaussian at $s = s_e$. Equations (D-5), (D-6), and the values of θ_{1_o} and θ_{2_o} completely specify the necessary boundary conditions for Eqs. (58) to (63).

REFERENCES

1. E. Silberman and H. Stefan, "Physical (Hydraulic) Modeling of Heat Dispersion in Large Lakes, a Review of the State of the Art," Univ. of Minn., St. Anthony Falls Hydraulic Lab., Project Report No. 115, 1970.
2. D. J. Baumgartner and D. S. Trent, "Ocean Outfall Design Part I: Literature Review and Theoretical Development," U.S. Dept. of Interior, Federal Water Quality Administration, 1970.
3. M. L. Albertson, Y. B. Dai, R. A. Jensen, and H. Rouse, "Diffusion of Submerged Jets," *ASCE Trans.*, **115**, 639–97 (1950).
4. S. Sami, T. Carmody, and H. Rouse, "Jet Diffusion in the Region of Flow Establishment," *J. Fluid Mech.* **27** (2), 231–52 (1967).
5. H. A. Becker, H. C. Hottel, and G. C. Williams, "The Nozzle-Fluid Concentration Field of the Round, Turbulent, Free Jet," *J. Fluid Mech.* **30**(2), 285–303 (1967).
6. I. Wygnanski and H. Fiedler, "Some Measurements in the Self Preserving Jet," *J. Fluid Mech.* **32**(2), 577–612 (1969).
7. W. Forstall and A. H. Shapiro, "Momentum and Mass Transfer in Coaxial Gas Jets," *J. Appl. Mech.* **17**, 399–408 (1950).
8. F. Landis and A. H. Shapiro, "The Turbulent Mixing of Co-axial Gas Jets," Heat Transfer and Fluid Mechanics Institute, 1951.
9. J. O. Hinze, *Turbulence*, McGraw-Hill, 1959.
10. G. N. Abramovich, *The Theory of Turbulent Jets*, translation by Scripta Technica, MIT Press, 1963.
11. H. Rouse, C. S. Yih, and H. W. Humphreys, "Gravitational Convection from a Boundary Source," *Tellus*, **4**, 201–210 (1952).
12. G. Abraham, "Entrainment Principle and Its Restrictions to Solve Problems of Jets," *J. Hydraulic Res.* 3(2), 1–23 (1965).
13. G. Abraham, "Jet Diffusion in Stagnant Ambient Fluid," Delft Hydraulics Lab. No. 29, 1963.
14. G. Abraham, "Jet Diffusion in Liquid of Greater Density," *ASCE J. Hydraulics Div.* **86**, HY6, 1–13 (1960).
15. R. J. Frankel and J. D. Cumming, "Turbulent Mixing Phenomena of Ocean Outfalls," *ASCE J. Sanit. Eng. Div.* **91**, SA2, 33–59 (1965).
16. W. E. Hart, "Jet Discharge into a Fluid with a Density Gradient," *ASCE J. Hydraulics Div.* **87**, HY6, 171–200 (1961).
17. T. V. Crawford and A. S. Leonard, "Observations of Buoyant Plumes in Calm Stably Stratified Air," *J. Appl. Meteorol.*, **1**, 251–56 (1962).
18. G. Abraham and W. D. Eysink, "Jets Issuing into Fluid with a Density Gradient," *J. Hydraulic Res.* 7(2), 145–75 (1969).
19. D. G. Fox, "Forced Plume in a Stratified Fluid," *J. Geophys. Res.* **75**(33), 6818–35 (1970).
20. L. N. Fan, "Turbulent Buoyant Jets into Stratified or Flowing Ambient Fluids," Keck Lab. of Hydraulics and Water Resources, CIT, Rept. No. KH-R-15, 1967.
21. C. H. B. Priestley and F. K. Ball, "Continuous Convection from an Isolated Source of Heat," *Quart. J. Roy. Meteorol. Soc.* **81**, 144–57 (1955).
22. F. H. Schmidt, "On the Diffusion of Heated Jets," *Tellus* **9**, 378–83 (1957).
23. B. R. Morton, A. G. Taylor, and J. S. Turner, "Turbulent Gravitational Convection from Maintained and Instantaneous Sources," *J. Roy. Soc. London* **A234**, 1–23 (1956).
24. K. Cederwall, "The Initial Mixing on Jet Disposal into a Recipient," Chalmers Univ. of Tech., Goteborg, Sweden, 1963 (in Swedish).
25. C. H. Bosanquet, G. Horn, and M. W. Thring, "The Effect of Density Differences on the Path of Jets," *J. Roy. Soc. London* **A263**, 340–52 (1961).
26. H. O. Anwar, "Behavior of Buoyant Jet in Calm Fluid," *ASCE J. Hydraulics Div.* **95**, HY4, 1289–1303 (1969).
27. G. Abraham, "Horizontal Jets in Stagnant Fluid of Other Density," *ASCE J. Hydraulics Div.* **91**, HY4, 139–53 (1965).
28. R. L. Gordier, "Studies on Fluid Jets Discharging Normally into Moving Liquid," Univ. of Minn., St. Anthony Falls Hydraulic Lab., Tech. Paper No. 28, Series B, 1959.
29. J. F. Keffer and W. D. Baines, "The Round Turbulent Jet in a Cross-Wind," *J. Fluid Mech.* 15(4), 481–97 (1963).
30. B. D. Pratte and W. D. Baines, "Profiles of the Round Turbulent Jet in a Cross Flow," *ASCE J. Hydraulics Div.* **93**, HY6, 53–64 (1967).
31. J. L. Platten and J. F. Keffer, "Entrainment in Deflected Axisymmetric Jets at Various Angles to the Stream," Univ. of Toronto, Mechanical Engineering Dept., UTME-TP-6808, 1968.
32. R. J. Margason, "The Path of a Jet Directed at Large Angles to a Subsonic Free Stream, NASA TN D-4919, 1968.

33. "Analysis of a Jet in a Subsonic Crosswind," Symposium Held at Langley Research Center, NASA SP-218, September 1969.

34. G. A. Briggs, *Plume Rise,* USAEC Division of Technical Information, 1969.

35. D. P. Hoult, J. A. Fay, and L. J. Forney, "A Theory of Plume Rise Compared with Field Observations," *J. Air Pollut. Contr. Ass.* **19**(9), 585–90 (1969).

36. J. A. Fay, M. Escudier, and D. P. Hoult, "A Correlation of Field Observations of Plume Rise," *J. Air Pollut. Contr. Ass.* **20**(6), 391–97 (1970).

37. D. P. Hoult and J. C. Weil, "Turbulent Plume in a Laminar Cross Flow," MIT Fluid Mechanics Lab., Publication No. 70-8, 1970.

38. F. W. Thomas, S. B. Carpenter, and W. C. Colbaugh, "Plume Rise Estimates for Electric Generating Stations," *Phil. Trans. Roy. Soc. London* **A-256**, 221-43 (1969).

39. "Full-Scale Study of Plume Rise at Large Electric Generating Stations," Tennessee Valley Authority, 1968.

40. B. Bringfelt, "Plume Rise Measurements at Industrial Chimneys," *Atmos. Environ.* **2**, 575–98 (1968).

41. T. A. Hewett, J. A. Fay, and D. P. Hoult, "Laboratory Experiments of Smokestack Plumes in a Stable Atmosphere," MIT Fluid Mechanics Lab., Publication No. 70-9, 1970.

42. J. W. Telford, "The Convective Mechanism in Clear Air," *J. Atmos. Sci.* **23**, 652-66 (1966).

43. R. B. Bird, W. E. Stewart, and E. N. Lightfoot, *Transport Phenomena,* Wiley, 1960.

44. J. N. Hunt, *Incompressible Fluid Dynamics,* Wiley, 1964.

45. H. Schlichting, *Boundary-Layer Theory,* 6th ed., McGraw-Hill, 1968.

46. S. Corrsin and A. L. Kistler, "The Free-Stream Boundaries of Turbulent Flows," NACA Report 1244, 1955.

47. J. S. Sastry and A. Okubo, "On the Prediction of the Probable Distribution of Concentration from Hypothetical Radioactive Sources on the Continental Slope off the East Coast of the U.S.," Reference 68-1, Chesapeake Bay Institute, 1968.

48. D. A. Thomson, A. R. Mead, and J. R. Schreiber, Jr., "Environmental Impact of Brine Effluents on Gulf of California," U.S. Dept. of Interior OSW R&D Progress Report No. 387, 1969.

49. R. F. Cayot and W. J. North, "Oceanographic Background Study: Diablo Canyon Nuclear Power Plant Site, Pacific Gas & Electric Co., San Francisco, Calif., 1967.

50. R. L. Wiegel, *Oceanographical Engineering,* Prentice-Hall, Inc., 1964.

51. T. D. Anderson, "Offshore Siting of Nuclear Energy Stations," *Nucl. Safety* **12**(1), 9–14 (1971).

52. R. A. Cox, M. J. McCartney, and F. Culkin, "The Specific Gravity/Salinity/Temperature Relationship in Natural Sea Water," *Deep-Sea Res.* **17**, 679–89 (1970).

53. W. B. Zerbe and C. B. Taylor, "Sea Water Temperature and Density Reduction Tables," U.S. Dept. of Commerce, Coast & Geodetic Survey No. 298, 1953.

54. M. R. Speigel, *Theory and Problems of Vector Analysis,* Schaum's Outline Series, McGraw-Hill, 1959.

55. W. C. Reynolds, "Computation of Turbulent Flows – State-of-the-Art, 1970," Mechanical Engineering Department, Stanford University, Report MD-27, 1970.

ORNL-4685
UC-48 — Biology and Medicine

INTERNAL DISTRIBUTION

1. Biology Library
2–4. Central Research Library
5. ORNL — Y-12 Technical Library
Document Reference Section
6–39. Laboratory Records Department
40. Laboratory Records, ORNL R.C.
41. S. I. Auerbach
42. S. E. Beall
43. J. R. Buchanan
44. R. S. Carlsmith
45. F. H. Clark
46. C. C. Coutant
47. K. E. Cowser
48. F. L. Culler
49. J. H. Gibbons
50. R. P. Hammond
51. R. F. Hibbs
52–301. E. A. Hirst
302. H. W. Hoffman
303. J. L. Liverman
304. R. N. Lyon
305. B. L. Nichols
306. R. B. Parker
307. M. Siman-Tov
308. M. J. Skinner
309. W. G. Stockdale
310. D. A. Sundberg
311. D. G. Thomas
312. D. B. Trauger
313. G. U. Ulrickson
314. A. M. Weinberg
315. R. P. Wichner
316–340. M. M. Yarosh

EXTERNAL DISTRIBUTION

341. J. A. Swartout, Union Carbide Corporation
342–344. Director, Division of Reactor Licensing
345–346. Director, Division of Reactor Standards
347. Laboratory and University Division, AEC, ORO
348. Patent Office, AEC, ORO
349–537. Given distribution as shown in TID-4500 under Biology and Medicine category (25 copies — NTIS)